

UNIVERSITY FOR DEVELOPMENT STUDIES

**BLASIUS FLOW OF MAGNETOHYDRODYNAMIC MICROPOLAR FLUID
PAST A PERMEABLE
PLATE WITH THERMAL RADIATION**

BY

**AYANDO TIMOTHY
(BSc. Mathematics)
(UDS/MM/0017/13)**

**DISSERTATION SUBMITTED TO THE DEPARTMENT OF MATHEMATICS,
FACULTY OF MATHEMATICAL SCIENCES, UNIVERSITY FOR DEVELOPMENT
STUDIES IN PARTIAL FULFILLMENT OF THE REQUIREMENTS FOR THE
AWARD OF MASTER OF SCIENCE DEGREE IN MATHEMATICS**

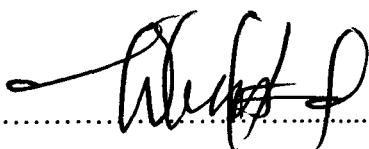
JULY, 2015



DECLARATION

Student

I hereby declare that this thesis is my original work and that no part of it has been presented for any degree in this university or elsewhere.

.....


Date: 31-10-2015

Ayando Timothy

Supervisor

I hereby declare that the preparation and presentation of this thesis was supervised in accordance with the guidelines on supervision of thesis laid down by the University for Development Studies:

.....


Date: 01/11/2015

Ing. Dr. Seini Yakubu Ibrahim



ABSTRACT

A mathematical investigation into the Blasius flow of an Magneto-HydroDynamics (MHD) micropolar fluid past a permeable flat plate with thermal radiation has been conducted. The governing boundary layer equations were modelled in the form of partial differential equations and transformed into ordinary differential equations using similarity analysis. The resulting higher order ordinary differential equations were then reduced to a system of first order differential equations and solved numerically using the Newton Raphson shooting method together with the forth-order Runge-Kutta integration scheme. The effects of embedded parameters on the fluid velocity, temperature profile, local skin friction coefficient, the rate of heat transfer (the local Nusselt number) and couple stresses in the flow regime have been depicted in tabular and graphical forms and discussed quantitatively. It was concluded from the study that, the magnetic field strength is the only embedded parameter that controls the flow kinematics and enhances the heat transfer process. In the same way, embedded parameters associated with thermal radiation, convective heating and viscous dissipation enhanced the heat transfer process.



ACKNOWLEDGEMENT

My first and foremost gratitude goes to the Almighty God for taking me through the 2-year course of study leading to this dissertation. He is the most powerful, compassionate, kind and merciful to all mankind.

Secondly, my heartfelt thanks go to Ing. Dr. Seini Yakubu Ibrahim for his time, patience and dedicated supervision. I always found him rich in new ideas. His genuine concern and friendship are irreplaceable. Finally, my profound appreciation goes to all my course mates and friends who have contributed in diverse ways to the success of this dissertation. God bless you all.



DEDICATION

To my lovely wife Bugase Georgina and children Cyprian and Reindolf.



TABLE OF CONTENTS

DECLARATION	i
ABSTRACT.....	ii
ACKNOWLEDGEMENT	iii
DEDICATION	iv
LIST OF TABLES	ix
LIST OF FIGURES	x
NOMENCLATURE	xii
CHAPTER ONE	1
INTRODUCTION	1
1.0 Introduction	1
1.1 Background to the Study	1
1.2 Statement of the Problem	3
1.3 Objectives of the Study	4
1.3.1 Main objective.....	4
1.3.2 Specific Objectives of the Study	4
1.4 Significance of the Study	5
1.5 Computational and Numerical Approach.....	5
1.6 Organization of the Study	6





CHAPTER TWO	7
REVIEW OF LITERATURE	7
2.0 Introduction.....	7
2.1 Micropolar Fluids.....	7
2.2 Stagnation Point Flows	9
2.3 Thermal Radiation on Flow Processes.....	10
2.4 Electromagnetic Effects of Fluid Flow	11
CHAPTER THREE	13
METHODOLOGY	13
3.0 Introduction.....	13
3.1 Basic Properties of Fluids	13
3.2 Formulation of Basic Mathematical Models.....	16
3.2.1 The Continuity Equation	16
3.2.2 The Navier-Stokes Equations.....	18
3.2.3 The Angular Momentum	24
3.2.4 The Energy Equation.....	26
3.3 Blasius flow of MHD micropolar fluid past a plate with thermal radiation	29
3.3.1 Modelling the Blasius Flow Problem.....	30
3.3.2 Dimensionless Governing Equations	31
3.3.3 The Similarity Variable	32



3.3.3 The Similarity Variable	32
3.3.4 The Stream Function	33
3.4 Transformation of the Modelled Equations	35
3.4.1 The Dimensionless Momentum Equation	36
3.4.2 The Dimensionless Energy Equation	37
3.4.3 Dimensionless Angular Momentum Equation	41
3.4.4 Dimensionless Boundary Conditions	42
CHAPTER FOUR.....	44
RESULTS AND DISCUSSIONS.....	44
4.0 Introduction	44
4.1 Numerical Procedure.....	44
4.2 Numerical Results	45
4.3 Order Reduction	45
4.4 Shear Stress, Couple Stress and Rates of Heat Transfer	47
4.5 Graphical Results	51
4.5.1 Velocity Profiles	51
4.4.2 Micro-rotation Profiles	56
4.4.3 Temperature Profiles	60
CHAPTER FIVE	66
CONCLUSIONS AND RECOMMENDATIONS.....	66

5.0 Introduction	66
5.1 Summary of Findings	66
5.3 Recommendations	68
5.4 Suggestion for further study	68
REFERENCES	70
APPENDICES	76
APPENDIX I	76
Fourth order Runge-Kutta and Newton-Raphson's algorithms	76
APPENDIX II	77
Maple code for numerical results	77
APPENDIX III	79
Maple code for graphical results	79



LIST OF TABLES

Table 4.1: Comparison of results of $f''(0)$ for varying values of Pr with $M = K = Br = Ra = 0, \lambda = 1$ and $Bi_x = 10^7$ 47

Table 4.2: Comparison of results of $-\theta(0)$ for varying values of Pr with $M = K = Br = Ra = 0, \lambda = 1$ and $Bi_x = 10^7$ 47

Table 4.3: Shear stress, Couple stress and Nusselt number under various parameters 49

Table 4.4: Numerical results of Shear stress and Nusselt number..... 50



LIST OF FIGURES

Figure 3.1: Mass flux through each of the six faces of a control volume of fluid 16

Figure 3.2: X-directional surface forces due to stress tensor component of a control volume..... 18

Figure 3.1: Schematic diagram of the problem.....30

Figure 4.1: Velocity profiles for varying values of magnetic field parameter.....52

Figure 4.2: Velocity profiles for varying values of suction parameter 52

Figure 4.3: Velocity profiles for varying values of Brinkmann Number 53

Figure 4.4: Velocity profiles for varying values of Biot number 54

Figure 4.5: Velocity profiles for varying/ values of material parameter 54

Figure 4.6: Velocity profiles for varying values of vortex viscosity parameter 55

Figure 4.7: Microrotation profiles for varying values of magnetic field parameter 56

Figure 4.8: Microrotation profiles for varying values of suction parameter.....57

Figure 4.9: Microrotation profiles for varying values of Brinkmann Number57

Figure 4.10: Microrotation profiles for varying values of Biot number 58

Figure 4.11: Microrotation profiles for varying values of vortex viscosity parameter 59

Figure 4.12: Microrotation profiles for varying values of vortex viscosity parameter 59

Figure 4.13: Temperature profiles for varying values of magnetic field parameter 60



Figure 4.14: Temperature profiles for varying values of suction parameter 61

Figure 4.15: Temperature profiles for varying values of the Prandtl number 61

Figure 4.16: Temperature profiles for varying values of the Brinkman number 62

Figure 4.17: Temperature profiles for varying values of Biot number 63

Figure 4.18: Temperature profiles for varying values of the radiation parameter 63

Figure 4.19: Temperature profiles for varying values of material parameter 64

Figure 4.20: Temperature profiles for varying values of material parameter 64



NOMENCLATURE

(x, y)	Cartesian coordinates
(u, v)	Velocity components in Cartesian Coordinates
C_s	Plate surface concentration
C_∞	Free stream concentration
C	Chemical species concentration
D	Diffusion coefficient
f	Dimensionless stream function
Nu	Nusselt number
T_∞	Free stream temperature
Sh	Sherwood number
T	Fluid temperature
Pr	Prandtl number
T_s	Plate surface temperature
κ	Thermal conductivity coefficient
K'	Mean absorption coefficient
Ra	Thermal radiation parameter
B_0	Constant magnetic field strength
γ	Reaction rate
q_r	Radiative heat flux
Ha_x	Hartmann number
Br	Brinkmann number
Bi_x	Local Biot number
Sc	Schmidt number



β_x	Local reaction rate parameter
Φ	Viscous dissipation function
f_w	Suction velocity
h_s	Heat transfer coefficient at plate surface

Greek Letters

μ	Coefficient of viscosity
ρ	Density of the fluid
ϕ	Dimensionless concentration
θ	Dimensionless temperature
η	Dimensionless variable
ν	Kinematic viscosity
ψ	Stream function
σ^*	Stefan-Boltzmann constant
σ	Electrical conductivity



CHAPTER ONE

INTRODUCTION

1.0 Introduction

This chapter presents the general introduction to the study. It provides a brief background leading to the problem statement. The general and specific objectives are stated as well as the significance of the study. It is concluded with the structure of the study.

1.1 Background to the Study

Fluid refers to any substance that has a tendency to deform continuously when subjected to shear stresses. Flow in pipes and channels, circulation of blood in vascular tumors, coating or spraying processes, flow of conducting fluids as well as flow under surface tension are all areas of active research. When fluid flows past objects, its molecules closer to the surface of the object is disturbed generating aerodynamic forces between the fluid and the object. As a result, molecules touching the surface directly stick to it while those particles located distances away are slowed down in their collisions with those sticking to the surface. These molecules in turn slow down the flow just above them such that molecules further away from the surface are least disturbed. Thus, a thin layer of fluid near the surface is set up in which the velocity changes from zero at the surface to the free stream value some distance away. Engineers called this the boundary layer as it occurs near the boundary of the object.

All fluids are basically classified into liquids or gases. Liquids are difficult to compress whereas gases are easily compressed and expand to fill their container. A gas has no free surface. The most important characteristic of a fluid from the viewpoint of fluid mechanics is its compressibility and viscosity. Fluid tends to flow when acted upon by





forces because they cannot resist the induced shearing effects. Prandtl (1904) observed that when fluid flow over a surface, its particles directly in touch with the surface move with it. Particles sticking to a stationary surface will thus have zero velocities. For gases, increased temperature makes the molecular movement more vigorous leading to increased molecular activity which increases the velocity near the surface.

In Newtonian fluids, the viscous stresses arising from the flow at every point is linearly proportional to the rate of change in deformation over time. Non-Newtonian fluids on the other hand have flow properties that differ in any way from those of the Newtonian fluids. Most commonly, the viscosity of non-Newtonian fluids is dependent on shear rate or shear rate history. Many salt solutions, molten polymers, ketchup, custard, toothpaste, starch suspensions, paints, blood and shampoo are examples of non-Newtonian fluids. In a non-Newtonian fluid, the relation between the shear stress and the shear rate is linear with the constant of proportionality being the coefficient of viscosity. The relation between the shear stress and the shear rate is different and can even be time dependent. Therefore a constant coefficient of viscosity cannot be defined.

Heat transfer processes basically occur in three forms namely; conduction, radiation, and convection. Conduction is the exchange of energy by direct interaction between molecules of a substance having temperature differences. It can occur in gases, liquids, or solids and has a strong basis in the molecular kinetic theory of Physics. Radiation is a transfer of thermal energy in the form of electromagnetic waves. Like electromagnetic radiation (light, X-rays, microwaves), thermal radiation travels with the speed of light, passing most easily through a vacuum or a nearly transparent gasses. Liquids containing



gases, such as carbon dioxide and water vapour, and glasses transmit only a portion of incident radiation, while most of solids are essentially opaque to radiation.

Convection remains the basic mode of heat transfer in fluids. It refers in general terms to the movement of molecules within fluids. Convective heat and mass transfer take place through both diffusion (the random Brownian motion of individual particles in the fluid) and by advection, in which matter or heat is transported by the larger-scale motion of currents in the fluid. In the context of heat and mass transfer, the term "convection" is used to refer to the sum of advective and diffusion.

Convection is the transfer of energy by conduction and radiation in moving fluid media. The motion of the fluid is an essential part of convective heat transfer. A key step in calculating the rate of heat transfer by convection is the calculation of the heat-transfer coefficient. In many cases of industrial importance, heat is transferred from one fluid, through a solid wall, to another fluid. The transfer often involves the use of heat exchangers.

1.2 Statement of the Problem

Many of the recent advances in science and technology are aimed at making devices smaller, effective and efficient. The electronic industry provides the best example of the gains in productivity, efficiency, scale and even new culture-changing products that result from designing and controlling small devices. Similar advances and applications in fluid dynamics are occurring at a rapid pace; the resulting technology is called Microfluidics. That is, when the typical sizes of the fluid-carrying channels are smaller than one millimeter. The theory of micropolar fluids is a special case of the theory of simple micro fluids. The ability to control flow kinematics in channels of such small dimensions

is leading to advances in basic research and technological innovations in biology, chemistry, engineering, and physics. The advances are most significant in research focusing on new materials, new fabrication methods, cooling of electronic devices, multiphase flows in labs-on-a-chip, and efforts to understand basic processes in individual biological cells. Among the techniques to control flow kinematics, the idea of using magnetic fields appear to be the most attractive because of its ease of implementation and its non-intrusive nature (Arthur *et al.*, 2014).

MHD micropolar fluid has received considerable attention of many researchers (Eringen, 2001) and (Ishak *et al.*, 2006) and the references therein. However, the combined effect of viscous dissipation and convective boundary condition on micropolar stagnation point flow over a porous surface in the presence of transverse magnetic field which often encountered in industry is limited.

1.3 Objectives of the Study

1.3.1 Main objective

To investigate the Blasius flow of MHD micropolar fluid combined with radiation, viscous dissipation and convective boundary conditions.

1.3.2 Specific Objectives of the Study

The specific objectives of the study are:

- i) To develop a mathematical model governing the flow of micropolar fluids.
- ii) To employ the techniques of similarity analysis to transform the modelled partial differential equations into ordinary differential equations.
- iii) To solve the transformed boundary value problem using numerical methods.





1.4 Significance of the Study

Understanding fluid dynamics in small devices led to advances in the study of micropolar fluid which is crucial to advances in science and engineering. For instance, modern engineering have led to an integrated system of thousands of small channels with hundreds of individually controlled valves into a single “lab-on-a-chip,” thus pointing the way to the kind of large-scale integration that transformed electrical circuit design and led to the computer revolution. These integrations produced more heat that led to the discovery of new heat transfer techniques. Understandably, research into heat transfer by MHD micropolar fluid has become a very important branch of fluid dynamics. This study will be of great importance in the design of systems or bodies in high speed flows and also in the design of thrust bearings and radial diffusers as well as in transpiration cooling and thermal oil recovery

1.5 Computational and Numerical Approach

The differential equations describing hydromagnetic boundary layer flow interaction with heat transfer over a flat surface constitute a nonlinear problem in an unbounded computational domain. The theory of nonlinear differential equations is quite elaborate and their solutions remain an extremely important problem of practical relevance in industrial and engineering systems. Approximate solutions for the nonlinear systems of differential equations modeling MHD flow over flat surfaces will be constructed using the fourth order Runge-Kutta integration scheme coupled with a numerical shooting technique. Numerical and graphical results will be presented and discussed quantitatively with respect to various parameters embedded in the problem.

1.6 Organization of the Study

The rest of the study is organized as follows: In Chapter Two of the study, we shall review relevant literature on micropolar fluids. Chapter Three presents the basic formulation of the generalized models, which are then applied to solve a specific problem of MHD micropolar fluid. Chapter Four then presents the results and discussions. Chapter Five presents the conclusions and recommendations of the study.



CHAPTER TWO

REVIEW OF LITERATURE

2.0 Introduction

This Chapter presents a review of related literature on micropolar fluids, which forms the bases for the study. It presents the research already done on micropolar fluids, stagnation point flows, thermal radiation on flow processes and finally the electromagnetic effects on fluid flow.

2.1 Micropolar Fluids

The classical Newtonian fluid model has not been adequate enough in describing some modern engineering and industrial processes involving materials with internal structure. Hoyt and Fabula (1964) experimentally investigated fluids that could not be characterized by the Newtonian model. Fluids having polymeric additives display more reduction of shear stresses and polymeric concentration as exhibited by Newtonian fluids (Eringen, 1965). The theory of micropolar fluids introduced by Eringen (1964, 1966) is one of the best theories that have been employed to describe the deformation of such materials.

Micropolar fluids are those consisting of randomly oriented particles suspended in a viscous medium, which can undergo rotation capable of affecting the hydrodynamics of the flow, making it a distinctly non-Newtonian fluid. They constitute an important branch of non-Newtonian fluid dynamics where micro-rotation effects as well as micro-inertia are exhibited. Eringen's theory has provided a good model for studying a number of complicated fluids such as colloidal fluids, polymeric fluids and blood.





Research into micropolar fluids has attracted the attention of many scientists mainly due to its important applications in industrial processes. These fluids find typical applications in colloidal flow, liquid crystals, lubricants, turbulent shear flow and flow in capillaries, heat exchangers, bubbly liquids, ferro-fluids, and even in the flow of blood in arteries, all of which contain intrinsic flow polarities.

The theoretical study of laminar flow over a flat plate as proposed by Blasius (1908) has been a cornerstone of fluid flow theories for many decades. Several wind tunnel results have consistently shown very good correspondence between the Blasius flow and experimental findings (Jovanovic *et al.*, 2006). The dynamics of micropolar fluids as originated from the theory of Eringen (1966) is an interesting area of fluid research. This theory explains the flow of colloidal suspensions (Hadimoto and Tokioka, 1969), liquid crystals, Lockwood *et al.*, (1987), polymeric fluids, human and animal blood, (Ariman *et al.*, 1974) among others.

Ahmadi (1976) proposed solutions for the flow of micropolar fluids past a semi-infinite plate while considering micro inertia effects. Soundalgekar and Takhar (1983) later studied the flow and heat transfer past a continuously moving plate in micropolar fluid whilst Rees and Pop (1998) analyzed the free convection boundary layer flow of micropolar fluids from a vertical flat plate. Ali and Hayat (2008) analyzed the peristaltic flow of a micropolar fluid in an asymmetric channel. Similarly, Sajid *et al.*, (2009) used the homotopy analysis method to examine the boundary layer flow of a micropolar fluid through a porous channel while Hayat and Ali (2008) investigated the effects of endoscope on peristaltic flow of micropolar fluid. Hayat *et al.* (2008) further examined the mixed convection flow of micropolar fluid over a non-linearly stretching sheet.

The two-dimensional flow of fluid near a stagnation-point is a classical problem in fluid dynamics. It plays a major role in industry particularly in the design of thrust bearings and radial diffusers, drag reduction, transpiration cooling and thermal oil recovery.

2.2 Stagnation Point Flows

The steady flow in the neighborhood of a stagnation-point was first studied by Hiemenz (1911) who employed the similarity techniques to transform the associated Navier-Stokes equations to non-linear systems of ordinary differential equations. This problem was extended by Homann (1936) to the case of axisymmetric stagnation-point flow. Later, the problem of stagnation point flow in two or three-dimensional cases were extended in numerous ways to include various physical effects.

MHD boundary layer flow is of considerable interest in the technical field due to its frequent occurrence in industrial technology and geothermal applications involving high-temperature plasmas applicable to nuclear fusion energy conversion, liquid metal fluids and MHD power generation systems. Nazar *et al.* (2004) studied the stagnation point flow of a micropolar fluid towards a stretching sheet whilst the MHD flow of micropolar fluid near a stagnation-point towards a non-linearly stretching surface was investigated by Hayat *et al.* (2009). Mahapatra and Gupta (2002) studied the heat transfer in the steady two dimensional stagnation-point flow of a viscous fluid by taking into account different aspects of the problem. Ishak *et al.* (2008) analyzed the MHD flow of a micropolar fluid towards a stagnation point on a vertical surface. Sparrow *et al.* (1961) earlier studied the effect of magnetic field on the natural convection heat transfer. Patel and Timol (2011) also studied the two-dimensional MHD stagnation-point flow of a power law fluid over a stretching surface. MHD flow of a micropolar fluid near a



stagnation-point towards a non-linear stretching surface was considered by Hayat (2009). Ibrahim and Makinde (2011) investigated the chemically reacting MHD boundary layer flow past a low-heat-sheet moving vertically downwards. Christian *et al.* (2014) examined the MHD boundary layer stagnation point flow with radiation and chemical reaction towards a heated shrinking porous surface.

2.3 Thermal Radiation on Flow Processes

The effect of thermal radiation on flow and heat transfer processes is of great importance in the design of many advanced energy conversion systems operating at high temperatures. Thermal radiations within such systems occur because of the emission by the hot walls into the working fluid. Many researchers have considered the radiation effects in their studies, Pop *et al.* (2004) and Zhu *et al.* (2011) among others.

Viscous dissipation plays an important role in various devices, which are subjected to large deceleration, in geological processes, polymer processing and also in strong gravitational field processes on large scales (on large planets) and has received considerable attention from researchers. Viscous dissipation changes the temperature distribution by playing a role of an energy source which leads to changes in the heat transfer rate. Subhas *et al.* (2007) studied viscoelastic MHD flow and heat transfer over a stretching sheet with viscous and ohmic dissipation. Makinde (2011) provided some similarity solutions for natural convection from a moving vertical plate with internal heat generation with convective boundary conditions. Lakshmi *et al.* (2012) examined the MHD boundary layer flow of heat and mass transfer over a moving vertical plate in a porous medium with suction and viscous dissipation. More recently, Arthur *et al.* (2014) investigated the chemically reacting hydromagnetic flow over a flat surface in the



presence of radiation with viscous dissipation and convective boundary conditions while Imoro *et al.* (2014), examined the heat and mass transfer over a vertical surface with convective boundary conditions in the presence of viscous dissipation and n^{th} order chemical reaction.

2.4 Electromagnetic Effects of Fluid Flow

The interaction of moving conducting fluids with electric and magnetic fields provide for a rich variety of phenomena associated with electro-fluid-mechanical energy conversion. Effects from such interactions can be observed in liquids, gases, two-phase mixtures, or plasmas. Numerous scientific and technical applications exist such as heating and flow control in metal processing, power generation from two-phase mixtures or seeded high-temperature gases, magnetic confinement of high-temperature plasmas-even dynamos that create magnetic fields in planetary bodies (Neil and Tillack, 1993). Several terms have been applied to this broad field of electromagnetic effects in conducting fluids, such as magneto-fluid- mechanics, magneto-gas-dynamics, and the more common one used here - magneto-hydrodynamics, or more simply as MHD.

MHD is the study of the dynamics of electrically conducting fluids such as plasmas, liquid metals and salt water or electrolyte. The fundamental concept behind MHD is that, magnetic fields can induce current in moving conductive fluid, which in turn creates forces on the fluid and also charges the magnetic field itself.

Incompressible fluid MHD was officially introduced in 1936 by Hannes Alfvén (1908-1995) who described astrophysical phenomena as an independent scientific discipline. Hartmann and Lazarus (1975), performed theoretical and experimental studies of MHD



flows in ducts. The most appropriate name for the phenomena would be “**Magneto Fluid Mechanics**,” but the original name “Magneto-hydrodynamics” is still generally used, (Abdou *et al.*, 2007). This study was conducted to investigate some aspects of MHD flow of micropolar fluids and apply the concepts to solve important problems faced by modern engineering and industrial practice.



CHAPTER THREE

METHODOLOGY

3.0 Introduction

The Chapter first provides some basic definitions of terms relevant to the study. A general model is derived and applied to solve a common industrial problem of micropolar fluids.

3.1 Basic Properties of Fluids

In studying the flow of fluids, some terms and definitions are often encountered. This section identifies such properties and briefly describes their importance and relevance.

i) Non-Linearity

All physical systems can be modelled in a form of nonlinear systems of differential equations. These nonlinearities in dynamical systems make solutions of most problems difficult to obtain. It is often necessary to approximate these non-linear equations to systems of linear equations by making some appropriate assumptions that allow direct solutions to be approximated. In fluid flow problems, nonlinearities are mostly due to the convective acceleration terms associated with the change of velocity over position. Thus, any convective flow, whether turbulent or not will involve nonlinearities.

ii) Density

Density (ρ) is defined as mass (m) per unit volume (V). That is,

$$\rho = \frac{m}{V} \quad (3.1)$$

The reciprocal of density is the **specific volume** (v), which is defined as volume per unit mass. The density of a substance, in general depends on temperature and pressure. The





density of most gases is proportional to pressure and inversely proportional to temperature. Liquids and solids, on the other hand, are essentially incompressible, and the variation of their density with pressure is usually negligible. The density of liquids and solids depends more strongly on temperature than it does on pressure.

iii) Viscosity

The velocity of fluid particles increase as the distance from the surface increases and reaches the maximum called the free stream value at a region far away from the object. The shearing stresses opposing the relative motion of fluid develop with magnitude depending on the velocity gradient from layer to layer. For fluids obeying Newton's law of viscosity, the x - coordinate is taken to act along the direction of flow with velocity, u . The shear stress (τ) in a fluid at a distance, y from the surface is given by:

$$\tau = \mu \frac{du}{dy} \quad (3.2)$$

Where μ is the co-efficient of dynamic viscosity defined as the shear force per unit area required to drag one layer of fluid with unit velocity past another layer a unit distance away from it in the fluid. The SI units for dynamic viscosity is the Newton- seconds per meter squared (Nsm^{-2})

iv) Kinematic Viscosity

The kinematic viscosity is defined as the ratio of the dynamic viscosity (μ) to the mass density. It is measured in squared meters per second (m^2s^{-1}) and mathematically expressed as

$$\nu = \frac{\mu}{\rho} \quad (3.3)$$



v). Internal Energy

The energy stored in a system due to the molecular interaction and bonding is referred to as the internal energy. A given mass of a viscous fluid may be viewed as a thermodynamic system that stores various forms of energies. The internal energy of a fluid includes the energy due to translation, rotation, vibration and the energy of molecular dissociation as well as energy of electronic excitation of the molecules. Internal energy has units of Jmol^{-1} .

vi) Thermal Conductivity

The thermal conductivity, κ is a measure of a material's ability to conduct heat. It relates the vector rate of heat transfer per unit area, q (also called the heat flux) to the vector gradient of temperature, ΔT . For solids and liquids the Fourier's law of heat conduction is given as:

$$q = -\kappa \nabla T, \tag{3.4}$$

where the negative sign indicates that heat flux is positive in the direction of decreasing temperature.

vii) Heat Transfer Coefficient

The local rate of convective heat transfer between a surface and the fluid is given by Newton's law of cooling

$$q = h_s (T_s - T), \tag{3.5}$$

Where h_s is the local heat transfer coefficient at the surface, T_s is the temperature of the surface, T is the bulk fluid temperature and q is the energy flux defined by Fourier's law given in equation (3.5).

3.2 Formulation of Basic Mathematical Models

The differential equations modelling the motion of a parcel of fluid through a controlled volume is obtained by applying the conservation laws of mass to a small volume of fluid. Consider the mass flux through each face of the fixed infinitesimal control volume shown in Fig 3.1 (Çengel and Cimbala,2006).

3.2.1 The Continuity Equation

The net flux of mass entering the element be equal to the rate of change of the mass of the element; that is,

$$\dot{m}_{in} - \dot{m}_{out} = \frac{\partial}{\partial t} m_{element} \quad (3.6)$$

To perform this mass balance, identify ρu , ρv and ρw at the centre of the element and then treat each of these quantities as a single variable.

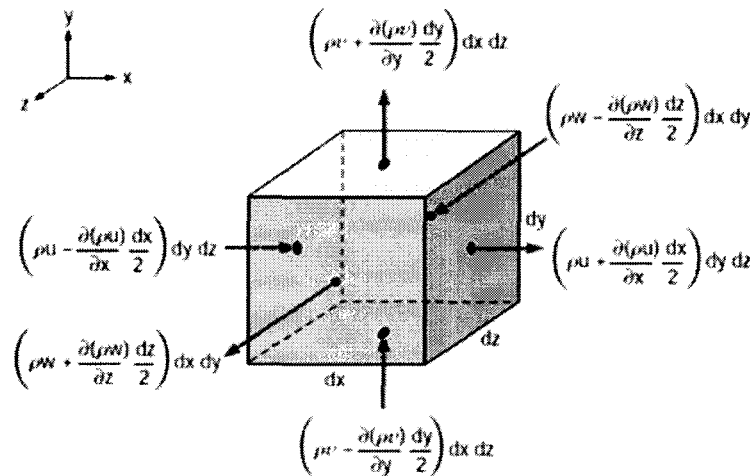


Figure 3.1 Mass flux through each of the six faces of a control volume of fluid

Figure 3.1 shows the mass flux through each of the six faces. Equation (3.6) then takes the form

$$\begin{aligned} & \left[\rho u - \frac{\partial(\rho u)}{\partial x} \frac{dx}{2} \right] dydz - \left[\rho u + \frac{\partial(\rho u)}{\partial x} \frac{dx}{2} \right] dydz + \left[\rho v - \frac{\partial(\rho v)}{\partial y} \frac{dy}{2} \right] dx dz - \left[\rho v + \frac{\partial(\rho v)}{\partial y} \frac{dy}{2} \right] dx dz \\ & + \left[\rho w - \frac{\partial(\rho w)}{\partial z} \frac{dz}{2} \right] dx dy - \left[\rho w + \frac{\partial(\rho w)}{\partial z} \frac{dz}{2} \right] dx dy = \frac{\partial}{\partial t} (\rho dx dy dz) \end{aligned} \quad (3.7)$$

Subtracting the appropriate terms and dividing by $dx dy dz$ gives,

$$\frac{\partial(\rho u)}{\partial x} + \frac{\partial(\rho v)}{\partial y} + \frac{\partial(\rho w)}{\partial z} = - \frac{\partial \rho}{\partial t} \quad (3.8)$$

Expanding and simplifying results in

$$\frac{\partial \rho}{\partial t} + u \frac{\partial \rho}{\partial x} + v \frac{\partial \rho}{\partial y} + w \frac{\partial \rho}{\partial z} + \rho \left(\frac{\partial u}{\partial x} + \frac{\partial v}{\partial y} + \frac{\partial w}{\partial z} \right) = 0 \quad (3.9)$$

In terms of substantial derivative, (3.9) can be written as

$$\frac{D\rho}{Dt} + \rho \left(\frac{\partial u}{\partial x} + \frac{\partial v}{\partial y} + \frac{\partial w}{\partial z} \right) = 0 \quad (3.10)$$

This is the most general form of the differential continuity equation expressed in rectangular coordinates. The gradient operator, ∇ called “del” can be introduced, which, in rectangular coordinates, is

$$\nabla = \frac{\partial}{\partial x} \hat{i} + \frac{\partial}{\partial y} \hat{j} + \frac{\partial}{\partial z} \hat{k} \quad (3.11)$$

The continuity equation can then be written in the form



$$\frac{D\rho}{Dt} + \rho \nabla \cdot V = 0 \quad (3.12)$$

Where $V = u\hat{i} + v\hat{j} + w\hat{k}$ and $\nabla \cdot V$ is called the divergence of the velocity. This form of the continuity equation is not limited to any particular coordinate system.

3.2.2 The Navier-Stokes Equations

The differential momentum equation is a vector equation in a scalar form. These component equations define the velocity and pressure fields. There are nine stress components of the stress tensor τ_{ij} that act at a particular point in a flow field. These stress tensors can be related to the velocity and the vector fields with the appropriate equations.

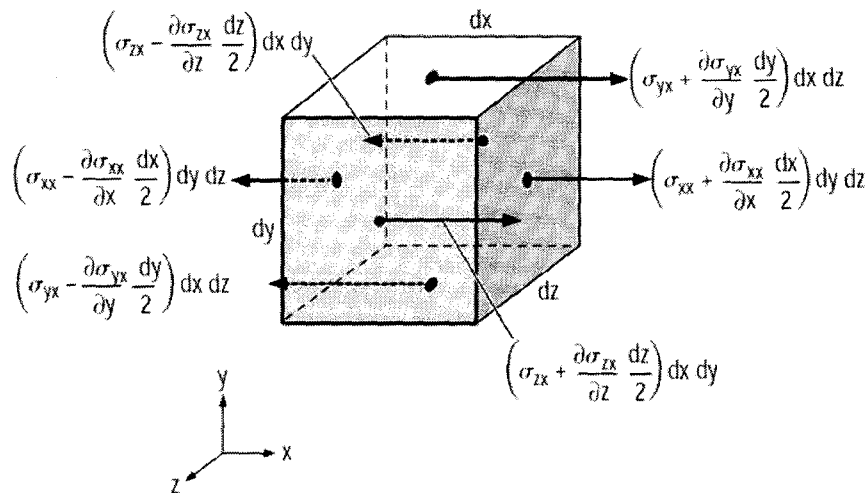


Figure 3.2. X-directional surface forces due to stress tensor component of a control volume

The stress components that act at a point are displayed on a two- and three-dimensional rectangular element shown in Figure 3.2 (Çengel and Cimbala, 2006). The element is





considered as an exaggerated point, a cubical point; the stress components act in the positive direction on a positive face (a normal vector point in the positive coordinate direction) and in the negative direction on a negative face (a normal vector points in the negative coordinate direction). The first subscript on a stress component denotes the face, upon which the component acts, and the second subscript denotes the direction in which it acts. Thus, the component τ_{xy} acts in the positive y -direction on a positive x -face.

A stress component that acts perpendicular to a face is referred to as a normal stress; the components σ_{xx} , σ_{yy} and σ_{zz} are normal stresses. A stress component that acts tangential to a face is called a shear stress; the components τ_{xy} , τ_{yx} , τ_{xz} , τ_{zx} , τ_{yz} and τ_{zy} are the shear stress components. There are nine stress components that act at a particular point in a fluid. The differential momentum equations are derived by considering the forces that act on the infinitesimal fluid particle. In Figure 3.2, only forces acting on the faces are shown. The stress components are assumed to be functions of x , y , z and t . Thus, the values of the stress components change from face to face since the location of each face is slightly different. The body force is shown acting in any arbitrary direction.

Newton's second law applied to a fluid particle, for the x -component direction, $\sum F_x = ma_x$. For the particle shown, it takes the form:

$$\left[\sigma_{xx} + \frac{\partial \sigma_{xx}}{\partial x} \frac{dx}{2} \right] dydz + \left[\tau_{yx} + \frac{\partial \tau_{yx}}{\partial y} \frac{dy}{2} \right] dx dz + \left[\tau_{zx} + \frac{\partial \tau_{zx}}{\partial z} \frac{dz}{2} \right] dx dy - \left[\sigma_{xx} - \frac{\partial \sigma_{xx}}{\partial x} \frac{dx}{2} \right] dydz - \left[\tau_{yx} - \frac{\partial \tau_{yx}}{\partial y} \frac{dy}{2} \right] dx dz - \left[\tau_{zx} - \frac{\partial \tau_{zx}}{\partial z} \frac{dz}{2} \right] dx dy + \rho g_x dx dy dz = \rho dx dy dz \frac{Du}{Dt}, \quad (3.13)$$

where the component of the gravity vector g in the x -direction is g_x and $\frac{Du}{Dt}$ is the x -component acceleration of the fluid particle. Dividing by the volume $dx dy dz$, (3.13) simplifies to

$$\rho \frac{Du}{Dt} = \frac{\partial \sigma_{xx}}{\partial x} + \frac{\partial \tau_{yx}}{\partial y} + \frac{\partial \tau_{zx}}{\partial z} + \rho g_x. \quad (3.14)$$

Similarly, for y - and z -directions, we have

$$\rho \frac{Dv}{Dt} = \frac{\partial \tau_{xy}}{\partial x} + \frac{\partial \sigma_{yy}}{\partial y} + \frac{\partial \tau_{zy}}{\partial z} + \rho g_y, \quad (3.15)$$

$$\rho \frac{Dw}{Dt} = \frac{\partial \tau_{xz}}{\partial x} + \frac{\partial \tau_{yz}}{\partial y} + \frac{\partial \sigma_{zz}}{\partial z} + \rho g_z. \quad (3.16)$$

We can show by taking moments about the axes passing through the centre of the infinitesimal element, that

$$\tau_{xy} = \tau_{yx}, \tau_{xz} = \tau_{zx}, \tau_{yz} = \tau_{zy} \quad (3.17)$$

That is, the stress tensor is symmetric; so there are actually six independent stress components. The stress tensor may be displayed in the usual way as

$$\tau_{ij} = \begin{pmatrix} \sigma_{xx} & \tau_{xy} & \tau_{xz} \\ \tau_{yx} & \sigma_{yy} & \tau_{yz} \\ \tau_{zx} & \tau_{zy} & \sigma_{zz} \end{pmatrix} \quad (3.18)$$

The subscripts i and j take on numerical values 1, 2, or 3. Then τ_{12} represents the element τ_{xy} in the first row and the second column.



Many fluids exhibit a linear relationship between the stress components and the velocity gradients. Such fluids are called Newtonian fluids and include common fluids such as water, oil, and air. If in addition to linearity, we require that the fluid be isotropic, it is possible to relate the stress components and the velocity gradients using only two fluid properties, the viscosity μ and the second coefficient of viscosity λ . The stress-velocity gradient relations, often referred to as the constitutive equations are given by Çengel and Cimbala (2006) as;

$$\begin{aligned}\sigma_{xx} &= -p + 2\mu \frac{\partial u}{\partial x} + \lambda \nabla \cdot V, \tau_{xy} = \mu \left(\frac{\partial u}{\partial y} + \frac{\partial v}{\partial x} \right), \\ \sigma_{yy} &= -p + 2\mu \frac{\partial v}{\partial y} + \lambda \nabla \cdot V, \tau_{xz} = \mu \left(\frac{\partial u}{\partial z} + \frac{\partial w}{\partial x} \right), \\ \sigma_{zz} &= -p + 2\mu \frac{\partial w}{\partial z} + \lambda \nabla \cdot V, \tau_{yz} = \mu \left(\frac{\partial v}{\partial z} + \frac{\partial w}{\partial y} \right).\end{aligned}\tag{3.19}$$

For most gases and for monatomic gases, the second coefficient of viscosity is related to the viscosity by

$$\lambda = -\frac{2}{3}\mu,\tag{3.20}$$

a condition known as Stokes' hypothesis. The negative average of the three normal stresses is equal to the pressure, that is,

$$-\frac{1}{3}(\sigma_{xx} + \sigma_{yy} + \sigma_{zz}) = p.\tag{3.21}$$

Using (3.19), this can be shown to always be true for a liquid in which $\nabla \cdot V = 0$, and with stokes' hypothesis, it is also true for a gas. If the constitutive equations are



substituted into the differential momentum equations (3.14), (3.15), and (3.16), there results, using Stokes' hypothesis,

$$\rho \frac{Du}{Dt} = -\frac{\partial p}{\partial x} + \rho g_x + \mu \left(\frac{\partial^2 u}{\partial x^2} + \frac{\partial^2 u}{\partial y^2} + \frac{\partial^2 u}{\partial z^2} \right) + \frac{\mu}{3} \frac{\partial}{\partial x} \left(\frac{\partial u}{\partial x} + \frac{\partial v}{\partial y} + \frac{\partial w}{\partial z} \right), \quad (3.22)$$

$$\rho \frac{Dv}{Dt} = -\frac{\partial p}{\partial y} + \rho g_y + \mu \left(\frac{\partial^2 v}{\partial x^2} + \frac{\partial^2 v}{\partial y^2} + \frac{\partial^2 v}{\partial z^2} \right) + \frac{\mu}{3} \frac{\partial}{\partial y} \left(\frac{\partial u}{\partial x} + \frac{\partial v}{\partial y} + \frac{\partial w}{\partial z} \right), \quad (3.23)$$

$$\rho \frac{Dw}{Dt} = -\frac{\partial p}{\partial z} + \rho g_z + \mu \left(\frac{\partial^2 w}{\partial x^2} + \frac{\partial^2 w}{\partial y^2} + \frac{\partial^2 w}{\partial z^2} \right) + \frac{\mu}{3} \frac{\partial}{\partial z} \left(\frac{\partial u}{\partial x} + \frac{\partial v}{\partial y} + \frac{\partial w}{\partial z} \right), \quad (3.24)$$

where a homogeneous fluid is assumed. That is, the fluid properties (for example, the viscosity) are independent of position. For an incompressible flow, these equations reduced to,

$$\rho \frac{Du}{Dt} = -\frac{\partial p}{\partial x} + \rho g_x + \mu \left(\frac{\partial^2 u}{\partial x^2} + \frac{\partial^2 u}{\partial y^2} + \frac{\partial^2 u}{\partial z^2} \right) \quad (3.25)$$

$$\rho \frac{Dv}{Dt} = -\frac{\partial p}{\partial y} + \rho g_y + \mu \left(\frac{\partial^2 v}{\partial x^2} + \frac{\partial^2 v}{\partial y^2} + \frac{\partial^2 v}{\partial z^2} \right) \quad (3.26)$$

$$\rho \frac{Dw}{Dt} = -\frac{\partial p}{\partial z} + \rho g_z + \mu \left(\frac{\partial^2 w}{\partial x^2} + \frac{\partial^2 w}{\partial y^2} + \frac{\partial^2 w}{\partial z^2} \right) \quad (3.27)$$

These are the Navier-Stokes Equations, named after Louis M. H. Navier (1785-1836) and George Stokes (1819-1903). The three differential equations together with the continuity equation give four equations and four unknowns in u , v , w and p . The viscosity and density are the fluid properties that can often be determined. With the appropriate





boundary and initial conditions, approximate solutions can be obtained. Several relatively simple geometries allow for analytical solutions.

Numerical solutions have also been determined for many flows of interest. Since the equations are in the form of nonlinear partial differential equations, it cannot be certain that the solution, obtained can exactly be realized in the laboratory. That is: the solutions are not unique. For example, a laminar flow and a turbulent flow may have the identical initial and boundary conditions, yet the two flows (the two solutions) are very different.

We can express the Navier-Stokes equations in vector form by multiplying (3.25), (3.26) and (3.27) by \hat{i} , \hat{j} and \hat{k} respectively, and adding recognizing that;

$$\begin{aligned}\frac{DV}{Dt} &= \frac{Du}{Dt} \hat{i} + \frac{Dv}{Dt} \hat{j} + \frac{Dw}{Dt} \hat{k}, \\ \nabla p &= \frac{\partial p}{\partial x} \hat{i} + \frac{\partial p}{\partial y} \hat{j} + \frac{\partial p}{\partial z} \hat{k},\end{aligned}\tag{3.28}$$

$$\nabla^2 V = \nabla^2 u \hat{i} + \nabla^2 v \hat{j} + \nabla^2 w \hat{k},$$

where the Laplacian is defined as:

$$\nabla^2 = \frac{\partial^2}{\partial x^2} + \frac{\partial^2}{\partial y^2} + \frac{\partial^2}{\partial z^2}\tag{3.29}$$

Combining the above, the Navier-Stokes equations in (3.25), (3.26) and (3.27) take the vector form

$$\rho \frac{DV}{Dt} = -\nabla p + \rho g + \mu \nabla^2 V\tag{3.30}$$

3.2.3 The Angular Momentum

In classical mechanics, angular momentum is defined as the product of the vector position and momentum,

$$\underline{L} \equiv \underline{r} \times \underline{p} = \begin{vmatrix} \underline{i} & \underline{j} & \underline{k} \\ x & y & z \\ p_x & p_y & p_z \end{vmatrix} \quad (3.31)$$

Note that the angular momentum itself is a vector. The three Cartesian components of the angular momentum are:

$$L_x = yp_z - zp_y \quad L_y = zp_x - xp_z \quad L_z = xp_y - yp_x \quad (3.32)$$

We can measure the angular momentum of a particle in a given quantum state. Define the operators \hat{X} and \hat{P} associated respectively to the position and the momentum of the particle.

$$\hat{L} = \hat{X} \times \hat{P} \quad (2.33)$$

where $\hat{P} = -i\hbar\nabla$. Note that in order to define the angular momentum, we have to use the definitions for the position and momentum operators and the expression for angular momentum in classical mechanics. Equation (3.28) yields explicit expressions for the components of the angular momentum as differential operators:

$$\begin{aligned} \hat{L}_x &= -i\hbar \left(y \frac{\partial}{\partial z} - z \frac{\partial}{\partial y} \right), & \hat{L}_y &= -i\hbar \left(z \frac{\partial}{\partial x} - x \frac{\partial}{\partial z} \right), \\ \hat{L}_z &= -i\hbar \left(x \frac{\partial}{\partial y} - y \frac{\partial}{\partial x} \right) \end{aligned} \quad (3.34)$$

Equation (3.29) can be economically written as:



$$\hat{L}_i = -ih\varepsilon_{ijk}x_j \frac{\partial}{\partial x_k} \quad (3.35)$$

where we have to sum over the repeated indices.

$$\begin{aligned} \hat{L}_x \hat{L}_y &= -h^2 \left(y \frac{\partial}{\partial z} - z \frac{\partial}{\partial y} \right) \left(z \frac{\partial}{\partial x} - x \frac{\partial}{\partial z} \right) \\ &= -h^2 \left\{ y \frac{\partial}{\partial x} - yz \frac{\partial^2}{\partial z \partial x} - yx \frac{\partial^2}{\partial z^2} - z^2 \frac{\partial^2}{\partial y \partial x} + zx \frac{\partial^2}{\partial y \partial z} \right\}, \end{aligned}$$

Whilst,

$$\begin{aligned} \hat{L}_y \hat{L}_x &= -h^2 \left(z \frac{\partial}{\partial x} - x \frac{\partial}{\partial z} \right) \left(y \frac{\partial}{\partial z} - z \frac{\partial}{\partial y} \right) \\ &= -h^2 \left\{ zy \frac{\partial^2}{\partial x \partial z} - z^2 \frac{\partial^2}{\partial x \partial y} - xy \frac{\partial^2}{\partial z^2} + xz \frac{\partial^2}{\partial z \partial y} + x \frac{\partial}{\partial y} \right\} \end{aligned}$$

Note the usual properties of partial derivatives

$$\frac{\partial^2}{\partial x \partial z} = \frac{\partial^2}{\partial z \partial x}, \quad \text{etc} \quad (3.36)$$

we obtain on subtraction the desired result

$$[\hat{L}_x, \hat{L}_y] = h^2 \left(x \frac{\partial}{\partial y} - y \frac{\partial}{\partial x} \right) = ih\hat{L}_z \quad (3.37)$$



3.2.4 The Energy Equation

Most problems of interest in fluid mechanics do not involve temperature gradients. They do however involve flows in which temperature everywhere is constant. For such flows, it is not necessary to introduce the differential energy equation. There are situations, however, for both compressible and incompressible flows, in which temperature gradients are important, and for such flows the differential energy equation is necessary. The differential energy equation is derived neglecting viscous effects, an assumption that significantly simplifies the derivation. Since the shear stresses that result from viscosity are quite small for many applications, this assumption may be acceptable. These shear stresses do, however, account for the high temperatures that burn up satellites on re-entry to the atmosphere; if they are significant, they must be included in any analysis.

Consider the infinitesimal fluid element again shown in Figure 3.1. The heat transfer rate \dot{Q} through an area A is given by the Fourier's law of heat transfer, named after Jean B.J. Fourier (1768-1830):

$$\dot{Q} = -\kappa A \frac{\partial T}{\partial n}, \quad (3.38)$$

where n is the direction normal to the area, T is the temperature, and κ is the thermal conductivity, assumed to be constant. The rate of work done by a force is the magnitude of the force multiplied by the velocity in the direction of the force, that is,

$$\dot{W} = pAV, \quad (3.39)$$

where V is the velocity in the direction of the pressure force pA . The first law of thermodynamics applied to a fluid particle can be written as



$$\dot{Q} - \dot{W} = \frac{DE}{Dt}, \quad (3.40)$$

where D/Dt is used since we are following a fluid particle at the instant shown.

For a particle occupying the infinitesimal element of Figure 3.1, the relationships above leads to:

$$\begin{aligned} & \kappa dydz \left(\frac{\partial T}{\partial x} \Big|_{x+dx} - \frac{\partial T}{\partial x} \Big|_x \right) - \frac{\partial}{\partial x} (pu) dx dy dz + \kappa dx dz \left(\frac{\partial T}{\partial y} \Big|_{y+dy} - \frac{\partial T}{\partial y} \Big|_y \right) - \frac{\partial}{\partial y} (pv) dx dy dz \\ & + \kappa dx dy \left(\frac{\partial T}{\partial z} \Big|_{z+dz} - \frac{\partial T}{\partial z} \Big|_z \right) - \frac{\partial}{\partial z} (pw) dx dy dz = \rho dx dy dz \frac{D}{Dt} \left(\frac{u^2 + v^2 + w^2}{2} + gz + \tilde{u} \right), \end{aligned} \quad (3.41)$$

where \tilde{u} is the internal energy, E has included kinetic, potential and internal energy, and the z -axis is assumed vertical. Also, since the mass of a fluid particle is constant $\rho dx dy dz$ is outside the D/Dt -operator. Divide both sides by $dx dy dz$ to get:

$$\kappa \left(\frac{\partial^2 T}{\partial x^2} + \frac{\partial^2 T}{\partial y^2} + \frac{\partial^2 T}{\partial z^2} \right) - \frac{\partial}{\partial x} (pu) - \frac{\partial}{\partial y} (pv) - \frac{\partial}{\partial z} (pw) = \rho \frac{D}{Dt} \left(\frac{u^2 + v^2 + w^2}{2} + gz + \tilde{u} \right). \quad (3.42)$$

This can be rearranged as follows:

$$\begin{aligned} & \kappa \left(\frac{\partial^2 T}{\partial x^2} + \frac{\partial^2 T}{\partial y^2} + \frac{\partial^2 T}{\partial z^2} \right) - p \left(\frac{\partial u}{\partial x} + \frac{\partial v}{\partial y} + \frac{\partial w}{\partial z} \right) - u \frac{\partial p}{\partial x} - v \frac{\partial p}{\partial y} \\ & - w \frac{\partial p}{\partial z} = \rho u \frac{Du}{Dt} + \rho v \frac{Dv}{Dt} + \rho w \frac{Dw}{Dt} + \rho g \frac{Dz}{Dt} + \rho \frac{D\tilde{u}}{Dt}. \end{aligned} \quad (3.43)$$

The Euler's equations are applicable for this inviscid flow. Hence, the last three terms on the left hand side equal the first four terms on the right if we recognize that



$$\frac{Dz}{Dt} = \frac{\partial z}{\partial t} + u \frac{\partial z}{\partial x} + v \frac{\partial z}{\partial y} + w \frac{\partial z}{\partial z} = \omega, \quad (3.44)$$

since x, y, z and t are all independent variables. The simplified energy equation then takes the form

$$\rho \frac{D\tilde{u}}{Dt} = \kappa \left(\frac{\partial^2 T}{\partial x^2} + \frac{\partial^2 T}{\partial y^2} + \frac{\partial^2 T}{\partial z^2} \right) - p \left(\frac{\partial u}{\partial x} + \frac{\partial v}{\partial y} + \frac{\partial w}{\partial z} \right). \quad (3.45)$$

In vector form, this is expressed as

$$\rho \frac{D\tilde{u}}{Dt} = \kappa \nabla^2 T - p \nabla \cdot V \quad (3.46)$$

Before simplifying this equation for incompressible gas flow, it could be written in terms of enthalpy rather than internal energy. Using

$$\tilde{u} = h - \frac{p}{\rho}. \quad (3.47)$$

The energy equation now becomes

$$\rho \frac{Dh}{Dt} = \kappa \nabla^2 T + \frac{Dp}{Dt}. \quad (3.48)$$

Two special cases can be considered. First, for a liquid flow, the continuity equation requires that $\nabla \cdot V = 0$ and with $\tilde{u} = c_p T$, c_p being the specific heat capacity at constant pressure. Equation (3.48) becomes

$$\frac{DT}{Dt} = \alpha \nabla^2 T \quad (3.49)$$



where we have introduced the thermal diffusivity defined by

$$\alpha = \frac{\kappa}{\rho c_p} \quad (3.50)$$

If viscous effects are not negligible, the derivation would include the work input due to the shear stress components. This would add a term to the right-hand side of the differential energy equations above; this term is called the dissipation function Φ , which, in rectangular coordinates, is

$$\Phi = 2\mu \left[\left(\frac{\partial u}{\partial x} \right)^2 + \left(\frac{\partial v}{\partial y} \right)^2 + \left(\frac{\partial w}{\partial z} \right)^2 + \frac{1}{2} \left(\frac{\partial u}{\partial y} + \frac{\partial v}{\partial x} \right)^2 + \frac{1}{2} \left(\frac{\partial v}{\partial z} + \frac{\partial w}{\partial y} \right)^2 + \frac{1}{2} \left(\frac{\partial u}{\partial z} + \frac{\partial w}{\partial x} \right)^2 \right] \quad (3.51)$$

Therefore, the energy equation for incompressible fluid flow becomes

$$\frac{DT}{Dt} = \alpha \Delta^2 T + \Phi \quad (3.52)$$

where the left hand represents the convective term whilst the right hand side are respectively, the rate of heat diffusion to the fluid particles and the rate of viscous dissipation per unit volume.

3.3 Blasius flow of MHD micropolar fluid past a plate with thermal radiation

The mathematical models developed in section 3.2 are employed to investigate a particular engineering problem frequently encountered in industry. Relevant assumptions are made and a numerical procedure based on the forth-order Runge-Kutta algorithm used to solve the problem. In this section, the combined effects of magnetic field, thermal



radiation with microrotation on the Blasius flow of an electrically conducting micropolar fluid on a permeable surface is studied.

3.3.1 Modelling the Blasius Flow Problem

Consider an MHD stagnation point flow of an electrically conducting micropolar fluid impinging normally on a heated vertical plate. The flow is assumed to be two-dimensional and steady, viscous and incompressible. It is further assumed that the velocity of the flow external to the boundary U and the temperature T_w of the plate are proportional to the distance x from the stagnation point so that $U = ax$ and $T_w = bx$, where a and b are constants.

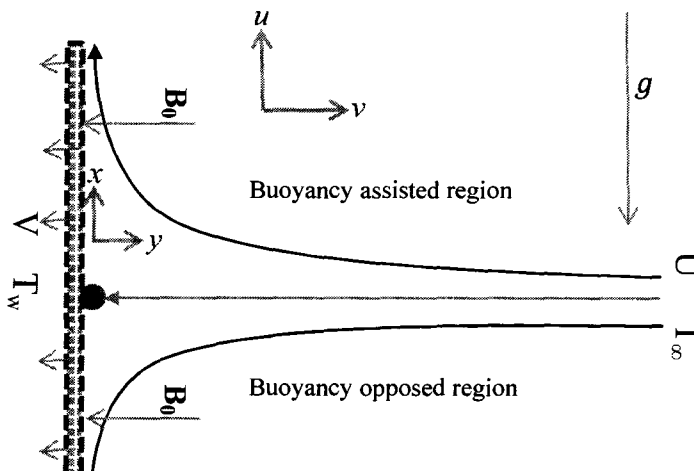


Figure 3.3: Schematic diagram of the problem

Following convection flow with heat transfer over a vertical plate in a stream of cold fluid at temperature T_∞ , it is also assumed that the left surface of the plate is heated by convection from a hot fluid at temperature T_w which provides a heat transfer coefficient



h_w . A uniform stationary magnetic field of strength B_0 is applied to the velocity field and the magnetic Reynolds number is assumed to be negligible. The induced magnetic field can be neglected as compared to the imposed magnetic field. It is further assumed that there is no applied polarization voltage, so the electric field is zero. Under these assumptions along with the Boussinesq and boundary layer approximations, the boundary layer equations modelling the flow is given by

$$\frac{\partial u}{\partial x} + \frac{\partial v}{\partial y} = 0, \quad (3.53)$$

$$u \frac{\partial u}{\partial x} + v \frac{\partial u}{\partial y} = U \frac{dU}{dx} + \left(\frac{\mu + k}{\rho} \right) \frac{\partial^2 u}{\partial y^2} + \frac{k}{\rho} \frac{\partial H}{\partial y} + \frac{\sigma B_0^2}{\rho} (u - U) + g\beta(T - T_\infty), \quad (3.54)$$

$$\rho j \left(u \frac{\partial H}{\partial x} + v \frac{\partial H}{\partial y} \right) = \gamma \frac{\partial^2 H}{\partial y^2} - k \left(2H + \frac{\partial u}{\partial y} \right), \quad (3.55)$$

$$\rho C_p \left(u \frac{\partial T}{\partial x} + v \frac{\partial T}{\partial y} \right) = \kappa \frac{\partial^2 T}{\partial y^2} + \sigma B_0^2 (u - U)^2 + \mu \left(\frac{\partial u}{\partial y} \right)^2 - \frac{\partial q_r}{\partial y}, \quad (3.56)$$

subject to boundary conditions:

$$y = 0: u = 0, v = -V, H = 0, \kappa \frac{\partial T}{\partial y} = -h_w (T_w - T),$$

$$y \rightarrow \infty: u \rightarrow U, H \rightarrow 0, T \rightarrow T_\infty, \quad (3.57)$$

3.3.2 Dimensionless Governing Equations

The similarity solution is based on the idea that the velocity and temperature distributions at any position along the plate surface, x , will collapse if plotted in dimensionless form as

a function of appropriately defined similarity variable. The similarity variable is defined as the ratio of the distance from the plate surface (y) to the approximate thickness of the momentum boundary layer (δ_m),

$$\eta = \frac{y}{\delta_m} \quad (3.58)$$

Therefore, the partial differential equations that describe the problem in terms of x and y will collapse to ordinary differential equations in η for dimensionless velocity, temperature and micro-rotation.

3.3.3 The Similarity Variable

The growth of the velocity and thermal boundary layers in a laminar flow occur primarily due to the molecular diffusion of momentum and energy. Therefore, the momentum boundary layer thickness (δ_m) will grow approximately according to:

$$\delta_m \approx 2\sqrt{\nu t},$$

where ν is the kinematic viscosity and t is time, which is related to the distance from the leading edge (x) and the characteristic velocity (u_{char}) according to:

$$t = \frac{x}{u_{char}}$$

In this study, the length is the total length of the plate (which is taken along the x -axis) while the characteristic velocity is the constant free-stream velocity far from the plate ($U_\infty = ax$). Thus,



$$\delta_m \approx 2\sqrt{\frac{\nu}{a}}$$

And
$$\eta = \frac{y}{2}\sqrt{\frac{a}{\nu}} \quad (3.59)$$

Following the presentation of Ostrach (1952), the constant used to define the similarity parameter is adjusted slightly, thus (3.59) becomes,

$$\eta = y\sqrt{\frac{a}{\nu}} \quad (3.60)$$

Hence (3.59) defines the similarity variable for the problem under investigation.

The dimensionless velocity and temperature fields are obtained from:

$$f' = \frac{u}{ax}, \quad \theta = \frac{T - T_\infty}{T_s - T_\infty} \quad (3.61)$$

At any position, x will collapse when expressed in terms of (3.60). Therefore,

$$f' = f'(x, y) = f'(\eta) \quad (3.62)$$

$$\theta = \theta(x, y) = \theta(\eta) \quad (3.63)$$

3.3.4 The Stream Function

The stream function is defined such that the continuity equation, (3.53), is automatically satisfied. That is,



$$u = \left(\frac{\partial \psi}{\partial y} \right)_x \text{ and } v = - \left(\frac{\partial \psi}{\partial x} \right)_y \quad (3.64)$$

The stream function is related to the volumetric flow Q between the surface of the plate and any position y according to,

$$Q = W\psi, \quad (3.65)$$

where W is the width of the plate . The volumetric flow rate is can be computed from the velocity field as:

$$Q = W \int_0^y u \, dy$$

This can be expressed in terms of the dimensionless variables (f' and η) as;

$$Q = aWx \sqrt{\frac{\nu}{a}} \int_0^\eta f' \, d\eta \quad (3.66)$$

Substituting Equation (3.66) into Equation (3.64) leads to:

$$\psi = ax \sqrt{\frac{\nu}{a}} \int_0^\eta f'(\eta) \, d\eta \quad (3.67)$$

The integral $\int_0^\eta f'(\eta) \, d\eta = f(\eta)$ in Equation (3.67) can be thought of as a dimensionless form of the stream function and must be a function of only the similarity variable (η).

Simplifying Equation (3.67) leads to:

$$\psi = \sqrt{av} \, xf(\eta)$$

This can be rewritten as: $\psi = x\sqrt{av}f(\eta)$ (3.68)



Equation (3.68) represents the stream function of the flow problem in this study.

3.4 Transformation of the Modelled Equations

The similarity variables are substituted into the governing x -momentum, angular momentum and thermal energy conservation equations as well as the boundary conditions for velocity, temperature and micro-rotation in order to transform the three coupled partial differential equations into three coupled ordinary differential equations that can readily be solved easily. The continuity equation is automatically satisfied using the stream function as defined. The transformation process involves taking the problem in terms of x and y and re-stating it in terms of η .

The similarity variable (3.59) is differentiated with respect to x and y to get;

$$\frac{\partial \eta}{\partial x} = 0, \quad \frac{\partial \eta}{\partial y} = \sqrt{\frac{a}{\nu}} \quad (3.69)$$

The x - component of velocity (u) is expressed in terms of the similarity variables as:

$$u = \frac{\partial \psi}{\partial y} = axf'(\eta) \quad (3.70)$$

Similarly, the y – component of velocity (v) in terms of the similarity variables is:

$$v = -\frac{\partial \psi}{\partial x} = -\sqrt{a\nu}f(\eta) \quad (3.71)$$

The partial derivatives of u with respect to x and y are obtained as follows:



$$\frac{\partial u}{\partial x} = af'(\eta), \quad \frac{\partial u}{\partial y} = a\sqrt{\frac{a}{\nu}}xf''(\eta), \quad \frac{\partial^2 u}{\partial y^2} = \frac{a^2}{\nu}xf'''(\eta) \quad (3.72)$$

The partial derivative of v with respect to y gives:

$$\frac{\partial v}{\partial y} = -af'(\eta) \quad (3.73)$$

The continuity equation is satisfied and therefore we proceed with the analysis to get the dimensionless momentum and energy equations.

3.4.1 The Dimensionless Momentum Equation

Substituting (3.72) and (3.73) into (3.54) gives,

$$axf'(\eta)(af'(\eta)) + -\sqrt{av}f\left(\sqrt{\frac{a^3}{\nu}}xf''(\eta)\right) = ax(a) + \left(\frac{\mu+k}{\rho}\right)\left(\frac{a^2x}{\nu}f'''(\eta)\right) + \frac{k}{\rho}\left(-\frac{a^2x}{\nu}h'(\eta)\right) + g\beta(T_w - T_\infty)\theta(\eta) - \frac{\sigma B_0^2}{\rho}(axf'(\eta) - ax)$$

Simplifying and grouping like-terms yields,

$$a^2xf'^2 - a^2xf''(\eta) = a^2x + a^2x\left(\frac{\mu+k}{\rho\nu}\right)f'''(\eta) - a^2x\left(\frac{k}{\rho\nu}\right)h'(\eta) + g\beta(T_w - T_\infty)\theta(\eta) - ax\frac{\sigma B_0^2}{\rho}(f'(\eta) - 1)$$

dividing through by a^2x and putting $\rho\nu = \mu$ gives,

$$f'^2 - ff''(\eta) = 1 + \left(1 + \frac{k}{\mu}\right)f'''(\eta) - \left(\frac{k}{\mu}\right)h'(\eta) + \frac{g\beta(T_w - T_\infty)}{a^2x}\theta(\eta) + \frac{\sigma B_0^2}{\rho a}(1 - f'(\eta)) \quad (3.74)$$



Noting that the coefficient $\frac{\sigma B_o^2}{\rho \alpha} = M$ is the magnetic field parameter, $\frac{k}{\mu} = K$ is the vortex viscosity parameter and $\frac{g\beta(T_w - T_\infty)}{a^2 x}$ which can be simplified further as $\lambda = Gr_x / Re_x^2$, represents the buoyancy or mixed convection parameter where $Gr_x = g\beta_T(T_w - T_\infty)x^3/\nu^2$ is the local thermal Grashof number and $Re_x = Ux/\nu$ is the local Reynolds number. Moreover, λ is a constant with $\lambda < 0$ and $\lambda > 0$ corresponds to the opposing and assisting buoyancy flows respectively, while $\lambda = 0$ is purely a forced convection flow.

Substituting these parameters and rearranging gives,

$$(1 + K)f'''(\eta) - f'^2 + ff''(\eta) + M(1 - f'(\eta)) - Kh'(\eta) + \lambda\theta(\eta) = 0 \quad (3.75)$$

This represents the dimensionless momentum equation which is a third-order non-linear ordinary differential equation.

3.4.2 The Dimensionless Energy Equation

To obtain the dimensionless energy equation for the flow problem, we write (3.61) as,

$$T = (T_w - T_\infty)\theta(\eta) + T_\infty \quad (3.76)$$

From the assumption that the temperature $T_w(x)$ at the wall is proportional to the distance x from the stagnation point, that is, $T_w = bx + T_\infty$, where b is constant. Thus (3.76) becomes,

$$T = bx\theta(\eta) + T_\infty \quad (3.77)$$

Finding the partial derivatives of (3.77) with respect to x and y yields,

$$\frac{\partial T}{\partial x} = b\theta(\eta), \quad \frac{\partial T}{\partial y} = \sqrt{\frac{a}{\nu}}bx\theta'(\eta), \quad \frac{\partial^2 T}{\partial y^2} = \frac{ab}{\nu}x\theta''(\eta) \quad (3.78)$$

For simplicity, the radiative heat flux term in the energy equation in (3.56) is analyzed by utilizing the Rosseland diffusion approximation (Sparrow, Cess and Timol, 1961) for an optically thick boundary layer flow as follows:

$$q_r = -\frac{4\sigma^*}{3K'} \frac{\partial T^4}{\partial y} \quad (3.79)$$

where K' and σ^* are the mean absorption coefficient and the Stefan-Boltzmann constant respectively. This approximation is valid at points optically far from the bounding surface, and it is good only for intensive absorption, that is, for an optically thick boundary layer (Pradeep and Hussain, 2001).

It is assumed that the temperature differences within the flow such as the term T^4 may be expressed as a linear function of temperature. Hence, expanding T^4 in a Taylor series about T_∞ and neglecting higher order terms leads to;

$$T^4 \cong 4T_\infty^3 T - 3T_\infty^4 \quad (3.80)$$

Differentiating (3.80) with respect to y gives,

$$\frac{\partial T^4}{\partial y} \cong 4T_\infty^3 \frac{\partial T}{\partial y}$$



Substituting into (3.79) gives:

$$q_r = -\frac{4\sigma^*}{3K'} * 4T_\infty^3 \frac{\partial T}{\partial y} \quad (3.81)$$

Differentiating (3.81) with respect to y gives,

$$\frac{\partial q_r}{\partial y} = -\frac{4\sigma^*}{3K'} * 4T_\infty^3 \frac{\partial^2 T}{\partial y^2} \quad (3.82)$$

The energy equation then transforms as;

$$\rho_c \left[axf'(\eta)(b\theta(\eta)) - \sqrt{av}f(\eta) \left(\sqrt{\frac{a}{v}}bx\theta'(\eta) \right) \right] = \frac{\kappa}{v} abx\theta''(\eta) + \mu \left(\sqrt{\frac{a^3}{v}}xf''(\eta) \right)^2 + \sigma B_o^2 (axf'(\eta) - ax)^2 + \frac{4\sigma^*T_\infty^3}{K'} \left(\frac{4ab}{3v}x\theta''(\eta) \right)$$

Expanding, dividing through by ρ_c and grouping like-terms in give,

$$abxf'(\eta)\theta(\eta) - abxf(\eta)\theta'(\eta) = \left(\frac{\kappa}{\rho_c} \right) \frac{ab}{v} x\theta''(\eta) + \frac{a^3\mu}{\rho_c v} x^2 f''^2(\eta) + \frac{a^2\sigma B_o^2}{\rho_c} x^2 (1 - f'(\eta))^2 + \frac{4\sigma^*T_\infty^3}{\rho_c K'} \left(\frac{4ab}{3v}x\theta''(\eta) \right)$$

Dividing through by $\left(\frac{\kappa}{\rho_c} \right) \frac{ab}{v} x$ and simplifying in yield,

$$\frac{\rho_c v}{\kappa} (f'(\eta)\theta(\eta) - f(\eta)\theta'(\eta)) = \theta''(\eta) + \frac{(ax)^2 \mu}{\kappa bx} f''^2(\eta) + \frac{\sigma B_o^2}{\rho_c a} \left(\frac{\mu(ax)^2}{\kappa bx} \right) (1 - f'(\eta))^2 + \frac{4\sigma^*T_\infty^3}{\kappa K'} \left(\frac{4}{3} \theta''(\eta) \right)$$



But $\frac{\kappa}{\rho c_p} = \alpha$ is the thermal diffusivity and $ax = U$ is the free stream velocity.

$$\frac{v}{\alpha} (f'(\eta)\theta(\eta) - f(\eta)\theta'(\eta)) = \theta''(\eta) + \frac{\mu U^2}{\kappa b x} f''^2(\eta) + \frac{\sigma B_0^2}{\rho a} \left(\frac{\mu U^2}{\kappa b x} \right) (1 - f'(\eta))^2 + \frac{4\sigma^* T_\infty^3}{\kappa K'} \left(\frac{4}{3} \theta''(\eta) \right)$$

Here the dimensionless parameters of the flow are: $Pr = \frac{v}{\alpha}$ is the Prandtl number;

$Ra = \frac{4\sigma^* T_\infty^3}{\kappa K'}$ is the thermal radiation parameter; $M = \frac{\sigma B_0^2}{\rho}$ is the local magnetic field

parameter; and $Br = \frac{\mu U_\infty^2}{\kappa b x}$ is the Brinkmann number. Thus,

$$Pr(f'(\eta)\theta(\eta) - f(\eta)\theta'(\eta)) = \theta''(\eta) + Br f''^2(\eta) + Br M (1 - f'(\eta))^2 + \frac{4}{3} Ra \theta''(\eta) \quad (3.83)$$

This can be rewritten as:

$$\left(1 + \frac{4}{3} Ra \right) \theta''(\eta) + Pr [f(\eta)\theta'(\eta) - f'(\eta)\theta(\eta)] + Br f''^2(\eta) + Br M (1 - f'(\eta))^2 = 0 \quad (3.84)$$

Equation (3.84) is the dimensionless thermal boundary layer equation. This is a second order nonlinear ordinary differential equation.



3.4.3 Dimensionless Angular Momentum Equation

For momentum we can write:

$$N = -a\sqrt{\frac{a}{\nu}}xh(\eta)$$

Finding the partial derivatives of with respect to x and y yields,

$$\frac{\partial N}{\partial x} = -a\sqrt{\frac{a}{\nu}}h(\eta), \quad \frac{\partial N}{\partial y} = -\frac{a^2}{\nu}xh'(\eta), \quad \frac{\partial^2 N}{\partial y^2} = -\frac{a^2}{\nu}\sqrt{\frac{a}{\nu}}xh''(\eta) \quad (3.85)$$

Substituting Equations (3.85) into (3.55) gives,

$$\begin{aligned} \rho j \left[axf'(\eta) \left(-a\sqrt{\frac{a}{\nu}}h(\eta) \right) - \sqrt{a\nu}f(\eta) \left(-\frac{a^2}{\nu}xh'(\eta) \right) \right] &= \gamma \left(\frac{a^2}{\nu}\sqrt{\frac{a}{\nu}}xh''(\eta) \right) - \\ k \left(-2a\sqrt{\frac{a}{\nu}}xh(\eta) + a\sqrt{\frac{a}{\nu}}xf''(\eta) \right) & \end{aligned} \quad (3.86)$$

Here $j = \nu/a$ represents the micro-inertia density and following the works of authors in literature, we assume that the spin gradient viscosity, $\gamma = (\mu + k/2)j = \mu(1 + K/2)j$, where $K = k/\mu$ is the vortex viscosity parameter. This assumption is made to allow the field of equations, predict the correct behaviour in the limiting case when the micro-structure effects become negligible and the total spin, H reduces to the angular velocity (see Ishak *et al.*, 2008). Expanding and grouping like terms in (3.86) give,

$$\begin{aligned} \rho \frac{\nu}{a} \left[-a^2 \sqrt{\frac{a}{\nu}}xf'(\eta)h(\eta) + a^2 \sqrt{\frac{a}{\nu}}xf(\eta)h'(\eta) \right] &= -\mu \left(1 + \frac{K}{2} \right) \left(\frac{\nu}{a} \right) \left(\frac{a^2}{\nu}\sqrt{\frac{a}{\nu}}xh''(\eta) \right) - \\ k \left(-2a\sqrt{\frac{a}{\nu}}xh(\eta) + a\sqrt{\frac{a}{\nu}}xf''(\eta) \right) & \end{aligned} \quad (3.87)$$



Dividing through by $-\rho\nu a\sqrt{\frac{a}{\nu}}x$ and simplifying in gives,

$$f'(\eta)h(\eta) - f(\eta)h'(\eta) = \left(1 + \frac{K}{2}\right)h''(\eta) + K(f''(\eta) - 2h(\eta))$$

The dimensionless parameter here is: $K = k/\mu$ is the vortex viscosity parameter

Simplifying further and rearranging in yield,

$$\left(1 + \frac{K}{2}\right)h''(\eta) + f(\eta)h'(\eta) - f'(\eta)h(\eta) + K(f''(\eta) - 2h(\eta)) = 0 \quad (3.88)$$

Equation (3.88) is the dimensionless angular momentum boundary layer equation. This is a second order nonlinear ordinary differential equation.

3.4.4 Dimensionless Boundary Conditions

The corresponding dimensionless boundary conditions are obtained by substituting the relevant terms into equation (3.56)

For the convective boundary condition, substitute the dimensionless temperature gradient

$$\text{into } -\kappa \frac{\partial T}{\partial y} = h_s(T_s - T).$$

That is,

$$-\kappa \frac{\partial T}{\partial y} \Big|_{y=0} = -\kappa \sqrt{\frac{a}{\nu}} (T_w - T_\infty) \theta'(0) = h_w [T_w - T]$$

Simplifying further by substituting (3.14) for T gives,



$$-\kappa \sqrt{\frac{a}{\nu}} (T_w - T_\infty) \theta'(0) = h_w [T_w - (T_w - T_\infty) \theta(0) - T_\infty]$$

Re-arranging for the dimensionless temperature gradient yields,

$$\theta'(0) = \frac{h_w}{\kappa} \sqrt{\frac{\nu}{a}} [\theta(0) - 1] \quad (3.89)$$

$Bi = \frac{h_w}{\kappa} \sqrt{\frac{\nu}{a}}$ represent the Biot number.

Hence, the convective boundary condition in dimensionless form is expressed as:

$$\theta'(0) = Bi[\theta(0) - 1] \quad (3.90)$$

The transformed boundary conditions are then stated as follows:

$$\begin{aligned} f(0) = fw, \quad f'(0) = 0, \quad \theta'(0) = Bi[\theta(0) - 1], \quad h(0) = 0, \\ f'(\infty) = 1, \quad \theta(\infty) = 0, \quad h(\infty) = 0. \end{aligned} \quad (3.91)$$

In the above equations, a prime denote the order of differentiation with respect to the similarity variable η and $fw = \frac{v}{\sqrt{av}}$ is the suction parameter.



CHAPTER FOUR

RESULTS AND DISCUSSIONS

4.0 Introduction

This chapter presents the results obtained through the analysis of the dimensionless coupled governing equations. The results are presented in both tables and graphical forms and discussed quantitatively for various parameter values.

4.1 Numerical Procedure

A numerical shooting technique based on the fourth-order Runge-Kutta integration algorithm was used to select a representative value for infinity, the similarity value can assume (η_{∞}), we begin with some initial guess value and solve the problem with some particular set of parameters to obtain $f''(0)$, $h'(0)$ and $\theta'(0)$. The solution process is repeated with another larger values of η_{∞} until two successive values of $f''(0)$, $h'(0)$ and $\theta'(0)$ differ only after a desired digit signifying the limit of the boundary along η . The last value of η_{∞} is chosen as appropriate value for that particular simultaneous equation of first order for seven unknowns following the method of superposition.

To solve this system we require seven initial conditions. There are only two initial conditions $f'(0)$ and $f(0)$ on f ; and one initial condition each on h and θ . This means that there are three initial conditions, $f''(0)$, $h'(0)$ and $\theta'(0)$ which are not specified. Now, we employ numerical shooting technique where these two ending boundary conditions are utilized to produce two unknown initial conditions at $\eta = 0$. In this calculation, the step size of $\Delta\eta = 0.001$ was used while obtaining the numerical solution with $\eta_{\max}=10$ and six-decimal (10^{-6}) accuracy as the criterion for convergence. The numerical procedure was carried out using a Maple 16 software package. A representative set of numerical results



are displayed graphically and discussed quantitatively to show some interesting aspects of some pertinent controlling parameters of the flow on the dimensionless axial velocity profiles, micro-rotation profiles, temperature profiles, shear stress, couple stress and the rate of heat transfer. The discussions of the results are also presented.

4.2 Numerical Results

From the process of numerical computation, the plate surface shear stress, couple stress and the local Nusselt number, which are respectively proportional to $f''(0)$, $h'(0)$ and $-\theta'(0)$ are computed from and their numerical values presented in tabular form. Tables 4.1 and 4.2 show the comparison of the works of Ramachandran *et al.* (1988), Lok *et al.* (2005) and Ishak *et al.* (2008) with the present study for various values of the Prandtl number (Pr). These numerical results were carried out using the fourth-order Runge-Kutta integration algorithm alongside a Maple 16 software package. It is clear from the table that the result of study is consistent with their works which validate the numerical approach adopted in this study.

4.3 Order Reduction

The transformed higher order ordinary differential equations obtained in equations (3.75), (3.84) and (3.88) and stated here for emphasis;

$$(1 + K)f'''(\eta) - f'^2 + ff''(\eta) + M(1 - f'(\eta)) - Kh'(\eta) + \lambda\theta(\eta) = 0$$

$$\left(1 + \frac{K}{2}\right)h''(\eta) + f(\eta)h'(\eta) - f'(\eta)h(\eta) + K(f''(\eta) - 2h(\eta)) = 0$$



$$\left(1 + \frac{4}{3} Ra\right) \theta''(\eta) + Pr[f(\eta)\theta'(\eta) - f'(\eta)\theta(\eta)] + Brf''^2(\eta) + BrM(1 - f'(\eta))^2 = 0$$

These equations are reduced to first order systems of differential equations.

From equation (3.75), Let $x_1 = f(\eta)$, $x_2 = f'(\eta)$, $x_3 = f''(\eta)$

From equation (3.84), Let $y_1 = h(\eta)$, $y_2 = h'(\eta)$,

From equation (3.88), Let $z_1 = \theta(\eta)$, $z_2 = \theta'(\eta)$

$$x_1' = x_2$$

$$x_2' = x_3$$

$$x_3' = \frac{1}{1+k} x_2^2 - \frac{1}{1+k} x_1 x_2 - \frac{M}{1+k} (1 - x_2) - \frac{k}{1+k} y_2 - \frac{\lambda}{1+k} z_1$$

$$y_1' = y_2$$

$$y_2' = \frac{1}{1+k/2} x_2 y_1 - \frac{1}{1+k/2} x_1 y_2 - \frac{k}{1+k/2} (x_3 - 2y_1)$$

$$z_1' = z_2$$

$$z_2' = \frac{Pr}{1 + \frac{4}{3} Ra} (x_2 z_1 - x_1 z_2) - \frac{Br}{1 + \frac{4}{3} Ra} x_3^2 - \frac{Br \cdot M}{1 + \frac{4}{3} Ra} (1 - x_2)^2$$

Applying the first order reduction to the boundary conditions is as follows:

$$x_1(0) = fw, \quad x_2(0) = 0, \quad z_2(0) = Bi[z_1(0) - 1]$$

$$y_1(0) = 0, \quad x_2(\infty) = 1, \quad z_1(\infty) = 0, \quad y_1(\infty) = 0$$

These reduced first order systems of differential equations was run on Maple 16 software for varying values of the Prandtl number when $M = K = Br = Ra = 0$, $\lambda = 1$ and $Bi_x = 10^7$ and the results compared to previous works of Ramachandran *et al.* (1988), Lok *et al.* (2005) and Ishak *et al.* (2008)



Table 4.1: Comparison of results of $f''(0)$ for varying values of Pr with $M = K = Br = Ra = 0, \lambda = 1$ and $Bi_x = 10^7$

Pr	Ramachandran <i>et al.</i> (1988)	Lok <i>et al.</i> (2005)	Ishak <i>et al.</i> (2008)	Present study
0.7	1.7063	1.706376	1.7063	1.7063226
1	-	-	1.6755	1.6754365
7	1.5179	1.517952	1.5179	1.5179126
10	-	-	1.4928	1.4928386

Table 4.2: Comparison of results of $-\theta(0)$ for varying values of Pr with $M = K = Br = Ra = 0, \lambda = 1$ and $Bi_x = 10^7$

Pr	Ramachandran <i>et al.</i> (1988)	Lok <i>et al.</i> (2005)	Ishak <i>et al.</i> (2008)	Present study
0.7	0.7641	0.764087	0.7641	0.7640633
1	-	-	0.8708	0.8707785
7	1.7224	1.722775	1.7225	1.7223813
10	-	-	1.9448	1.9446170

4.4 Shear Stress, Couple Stress and Rates of Heat Transfer

The effects of varying parameter values on the shear stress, couple stress and the rate of heat transfer (local Nusselt number) are obtained from equations (3.75), (3.84), and (3.88) and shown in Table 4.3. It is observed that both the shear and couple stresses increase with increasing values of M, fw, Br, Bi, Ra and λ ($\lambda > 0$); and decreases with increasing values of Pr, K and λ ($\lambda < 0$). This means that the combined effect of magnetic



field intensity, suction, viscous dissipation, convective heat transfer, thermal radiation, and buoyancy force due to assisting flow is to increase the shear and couple stresses; and the combined effect of the linear momentum diffusion, angular momentum diffusion and buoyancy force due to opposing flow is to decrease the shear and couple stresses at the surface of the plate.

On the other hand, the rate of heat transfer at the plate surface increases with Pr , f_w and Bi numbers and reduces with increasing values of M , K , Br , Ra and λ . This means that the combined effect of the momentum diffusion, suction and convective heat transfer as well as the buoyancy force due to assisting flow is to increase the rate of heat transfer. Furthermore, the combined effect of the magnetic field intensity, micro-rotation diffusion, viscous dissipation, thermal radiation and buoyancy force due to both assisting and opposing flows is to decrease the shear and couple stresses at the surface of the plate.



Table 4.3: Shear stress, Couple stress and Nusselt number under various parameters

Pr	M	K	λ	Ra	Br	Bi	f_w	$f''(0)$	$h'(0)$	$-\theta'(0)$
0.7	0.1	1.0	1.0	0.1	0.1	0.1	0.1	0.957132	0.308024	0.081916
1.0	0.1	1.0	1.0	0.1	0.1	0.1	0.1	0.945768	0.305856	0.084270
7.0	0.1	1.0	1.0	0.1	0.1	0.1	0.1	0.910460	0.300194	0.093238
10.0	0.1	1.0	1.0	0.1	0.1	0.1	0.1	0.907330	0.299823	0.094352
0.7	0.5	1.0	1.0	0.1	0.1	0.1	0.1	1.062086	0.321666	0.080289
0.7	1.0	1.0	1.0	0.1	0.1	0.1	0.1	1.179707	0.335759	0.078528
0.7	0.1	2.0	1.0	0.1	0.1	0.1	0.1	0.745933	0.374231	0.082125
0.7	0.1	3.0	1.0	0.1	0.1	0.1	0.1	0.624275	0.386234	0.082127
0.7	0.1	1.0	-3.0	0.1	0.1	0.1	0.1	-0.451157	-0.063904	0.031934
0.7	0.1	1.0	-2.0	0.1	0.1	0.1	0.1	-0.445804	-0.078155	0.004750
0.7	0.1	1.0	1.0	0.1	0.1	0.1	0.1	0.957132	0.308024	0.081016
0.7	0.1	1.0	2.0	0.1	0.1	0.1	0.1	1.015643	0.316797	0.081817
0.7	0.1	1.0	1.0	0.5	0.1	0.1	0.1	0.963837	0.309628	0.081024
0.7	0.1	1.0	1.0	1.0	0.1	0.1	0.1	0.971236	0.311393	0.079943
0.7	0.1	1.0	1.0	1.0	0.5	0.1	0.1	1.039356	0.320988	0.059759
0.7	0.1	1.0	1.0	1.0	1.0	0.1	0.1	1.154654	0.338446	0.027177
0.7	0.1	1.0	1.0	1.0	0.1	0.5	0.1	1.039449	0.319955	0.270775
0.7	0.1	1.0	1.0	1.0	0.1	1.0	0.1	1.085869	0.382010	0.382020
0.7	0.1	1.0	1.0	1.0	0.1	0.1	0.5	1.070366	0.339993	0.084424
0.7	0.1	1.0	1.0	1.0	0.1	0.1	1.0	1.228099	0.378357	0.086757

Table 4.4 shows the computations of the shear stress and the rate of heat transfer at the surface for ($K=0, 1$) with various values of convection parameter (λ). With respect to the model, $K=0$ means Newtonian fluid whereas $K \neq 0$ ($K=1$ is used in this study) means non-Newtonian fluids. As shown in Table 4.4 for the Newtonian fluid case ($K=0$), the



shear stress increases and the rate of heat transfer reduces at the surface for increasing buoyancy force due to both assisting and opposing flows. Furthermore, for the non-Newtonian fluid case ($K \neq 0$), increasing the buoyancy force due to opposing flow reduces the skin friction and the rate of heat transfer at the surface whereas increasing the buoyancy force due to assisting flow increases the shear stress and reduces the rate of heat transfer at the surface.

Table 4.4: Numerical results of Shear stress and Nusselt number

Pr	M	Ra	Br	Bi	F_w	K	λ	$f''(0)$	$-\theta'(0)$
1.0	0.1	0.1	0.1	0.1	0.1	0	-3	-0.640149	0.035007
1.0	0.1	0.1	0.1	0.1	0.1	0	-2	-0.633822	0.008194
1.0	0.1	0.1	0.1	0.1	0.1	0	0	1.330132	0.083632
1.0	0.1	0.1	0.1	0.1	0.1	0	1	1.412149	0.083452
1.0	0.1	0.1	0.1	0.1	0.1	0	2	1.494733	0.083253
1.0	0.1	0.1	0.1	0.1	0.1	1	-3	-0.476468	0.028082
1.0	0.1	0.1	0.1	0.1	0.1	1	-2	-0.471736	0.001633
1.0	0.1	0.1	0.1	0.1	0.1	1	0	0.898236	0.084312
1.0	0.1	0.1	0.1	0.1	0.1	1	1	0.945768	0.084270
1.0	0.1	0.1	0.1	0.1	0.1	1	2	0.992927	0.084218



4.5 Graphical Results

4.5.1 Velocity Profiles

The effects of parameter variation on the velocity boundary layer are shown in Figures 4.1- 4.6. Normally, the fluid velocity is minimal at the plate surface and increases to the free stream value satisfying the far field boundary conditions. The effect of the Magnetic Parameter (M) on the velocity is shown in Figure 4.1. It is observed that a longitudinal decrease in the velocity accompanies a steady decrease in the magnetic field intensity. This is due to the fact that the applied magnetic field normal to the flow direction induces the drag in terms of a Lorentz force which provides resistance to flow.

For various values of suction parameter (f_w), the profiles of the velocity across the boundary layer are shown in Figure 4.2. The velocity decreases for increasing values of f_w . This can be attributed to the fact that suction is an agent which causes resistance to the fluid flow hence retarding the fluid velocity.



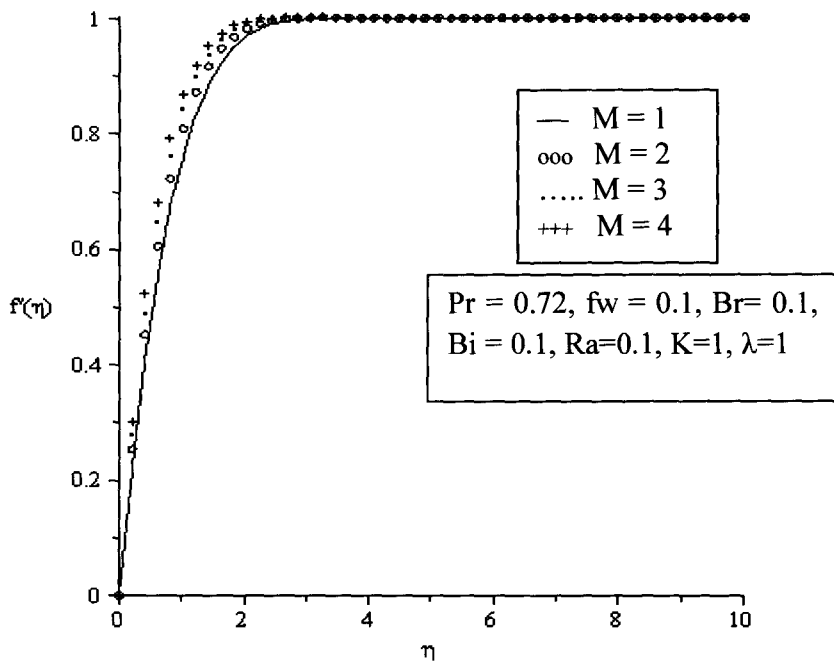


Figure 4. 1: Velocity profiles for varying values of magnetic field parameter

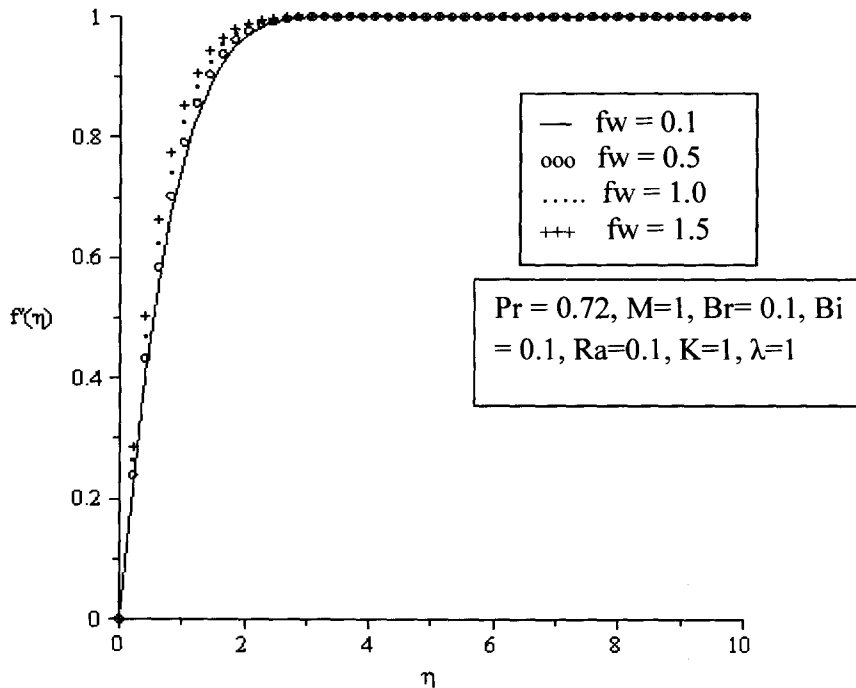


Figure 4. 2: Velocity profiles for varying values of suction parameter

Figures 4.3, 4.4 and 4.5 depict the effects of Brinkmann number (Br), Biot number (Bi) and thermal radiation parameter (Ra) respectively, on the dimensionless velocity. It is observed that increasing values of Br, Bi and Ra reduce the velocity at the surface of the plate and increase the free stream value due to rising buoyancy force as a result of viscous heating, convective heat transfer and thermal radiation respectively.

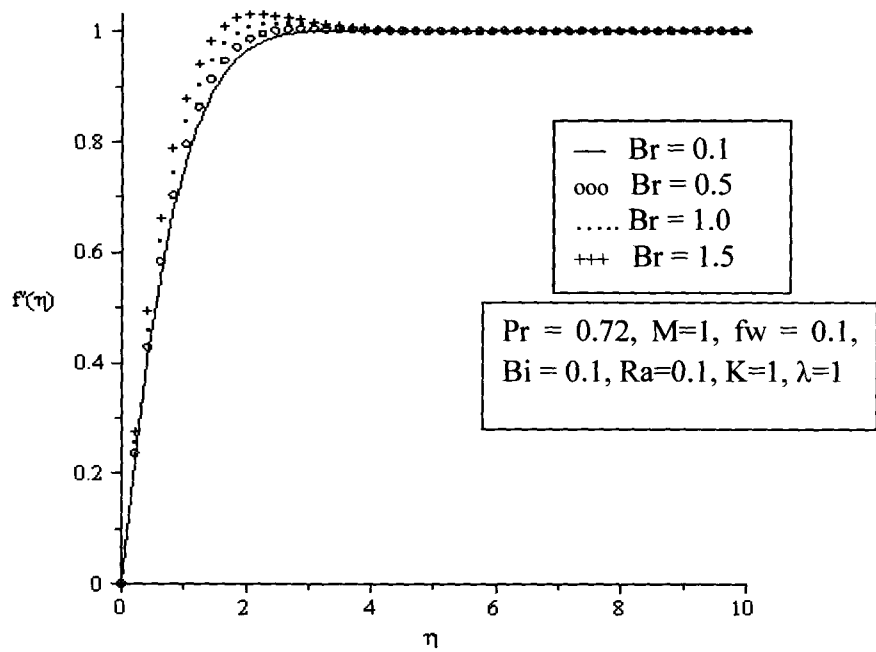


Figure 4. 3: Velocity profiles for varying values of Brinkmann Number

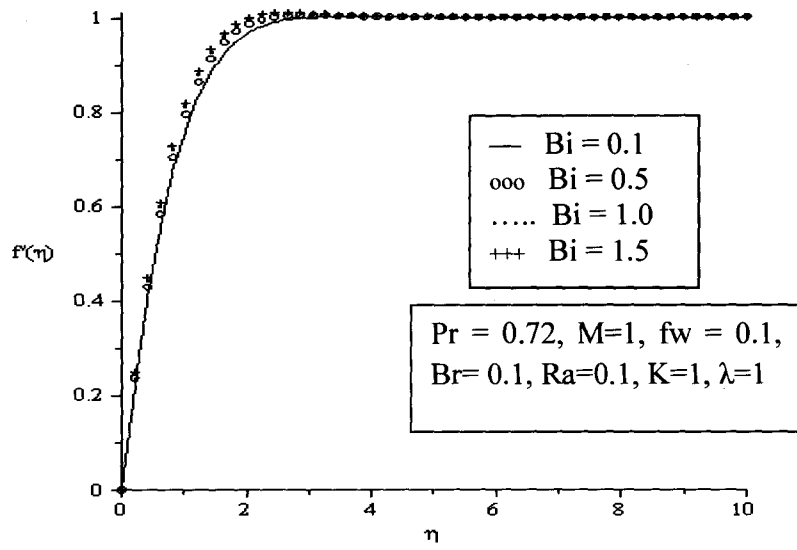


Figure 4. 4: Velocity profiles for varying values of Biot number

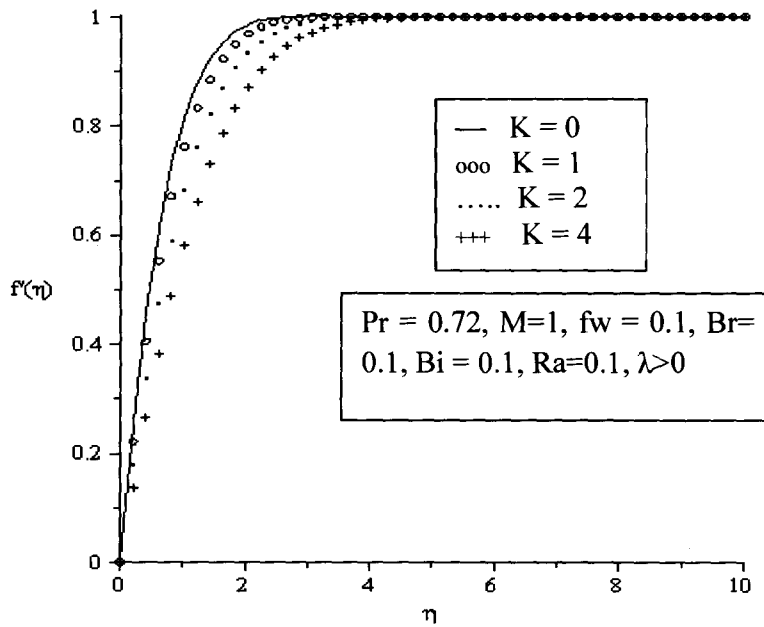


Figure 4. 5: Velocity profiles for varying/ values of material parameter (assisting flow)

Figure 4.6 represents the variation of different values of vortex viscosity parameter (K) on the dimensionless velocity distributions for assisting and opposing flows. It is observed that increasing the values of K for both assisting and opposing flows lead to a decrease in the fluid flow, which causes the momentum boundary layer thickness generally, to shrink away from the plate satisfying the far field boundary conditions. It therefore suffices here to say that, increases in angular momentum diffusion will lead to a better flow kinematics.

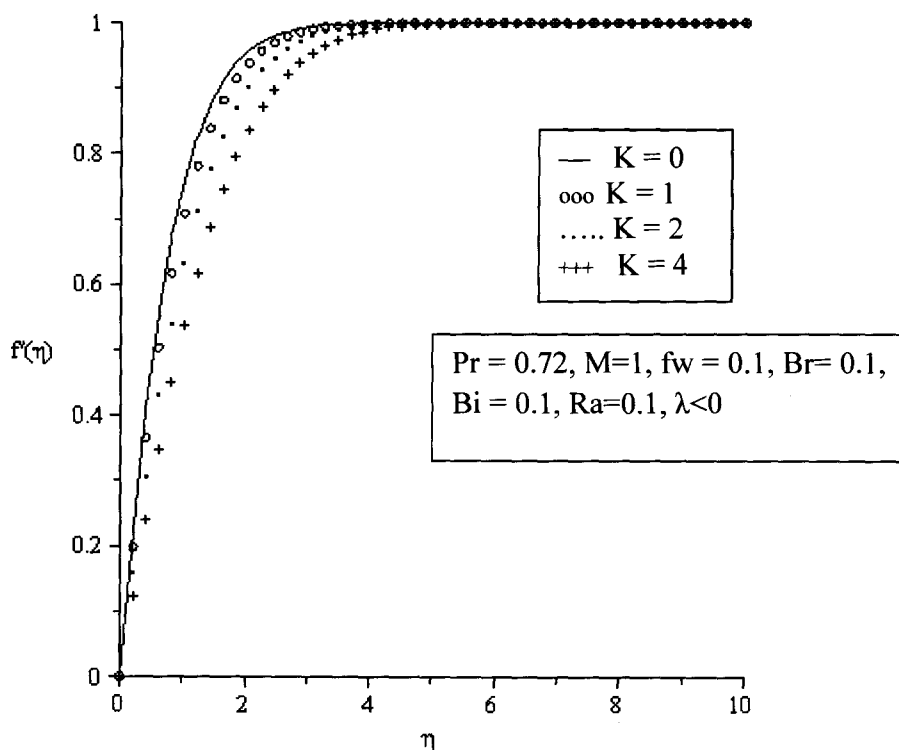


Figure 4. 6: Velocity profiles for varying values of vortex viscosity parameter (opposing flow)



4.4.2 Micro-rotation Profiles

The effects of parameter variation on the micro-rotation boundary layer are shown in Figures 4.7-4.12. Figures 4.7 and 4.8 show the effect of magnetic field and suction parameters respectively on the micro-rotation profiles. It is observed that a longitudinal decrease in micro-rotation profiles is accompanied by increasing values of both M and f_w . This can be attributed to the fact that increasing the magnetic field intensity induces the Lorenz force, which tends to increase the couple stress (Table 4.3) hence the longitudinal decrease in the micro-rotation.

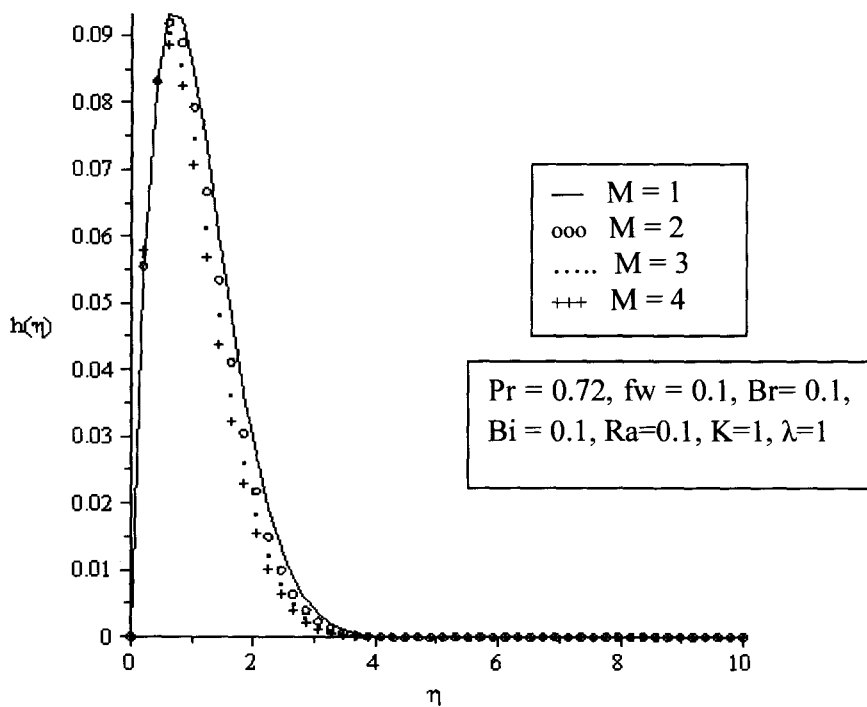


Figure 4. 7: Microrotation profiles for varying values of magnetic field parameter

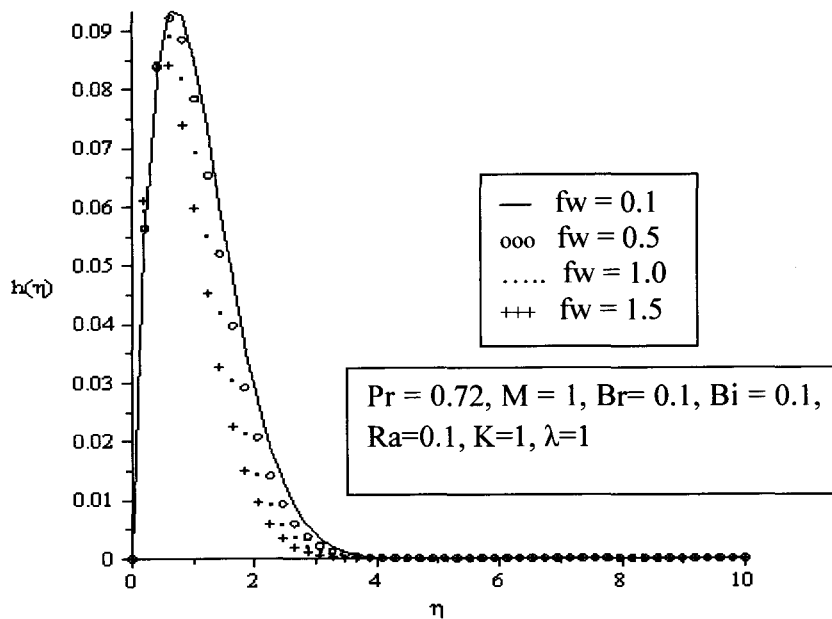


Figure 4. 8: Microrotation profiles for varying values of suction parameter

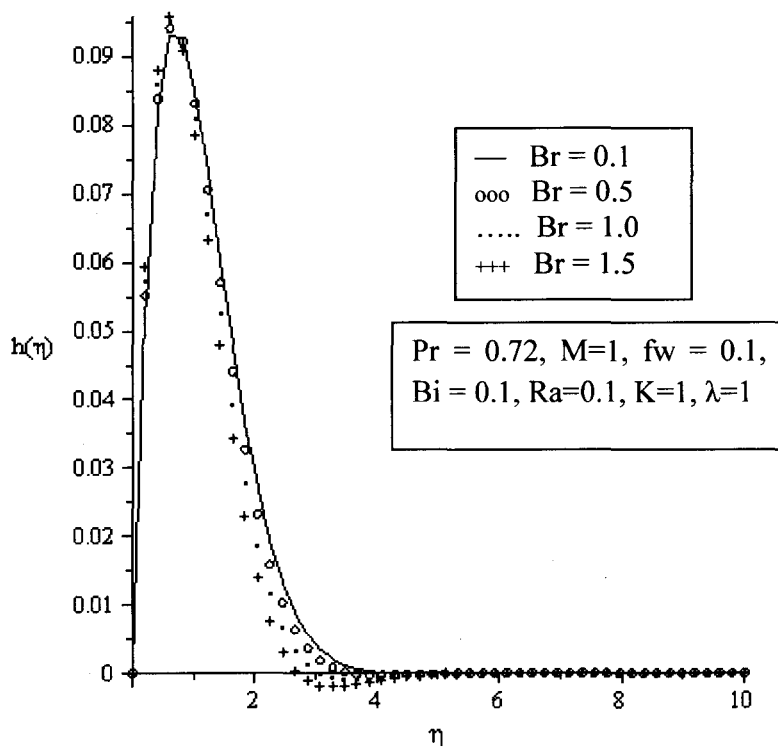


Figure 4. 9: Microrotation profiles for varying values of Brinkmann Number



Figures 4.10 and 4.11 show the effect of Brinkmann and Biot numbers respectively on the micro-rotation profiles. It is observed that increasing values of both parameters reduces the micro-rotation profiles at the surface of the plate and increases the free stream thereof. This is due to the fact that in increasing Br and Bi , internal heat rises due to viscous dissipation and convective heat transfer leading to buoyancy effects.

Figures 4.12 and 4.13 depict the effect of vortex viscosity parameter for assisting and opposing flows respectively. It is observed that increasing values of the vortex viscosity increases microrotation profiles at the surface of the plate and reduces to free stream for both flows, due to a rise in angular momentum diffusion.

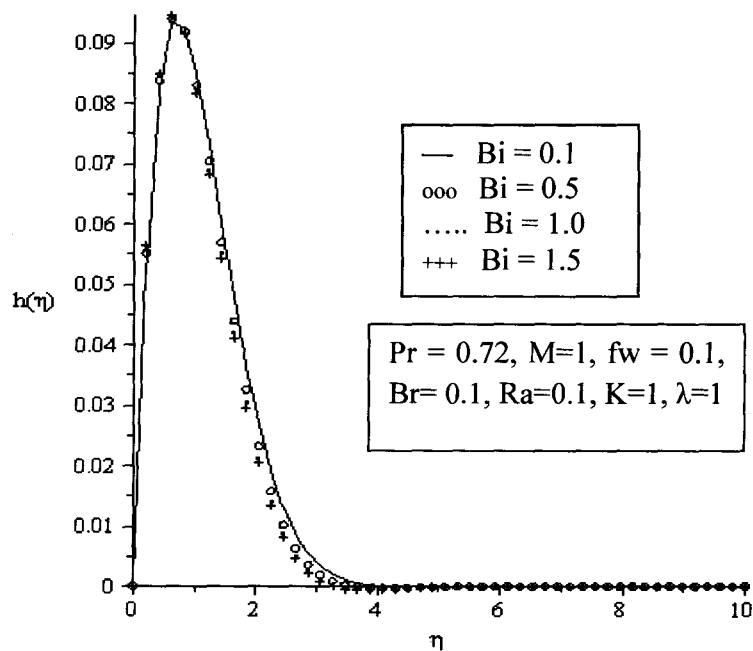


Figure 4. 10: Microrotation profiles for varying values of Biot number

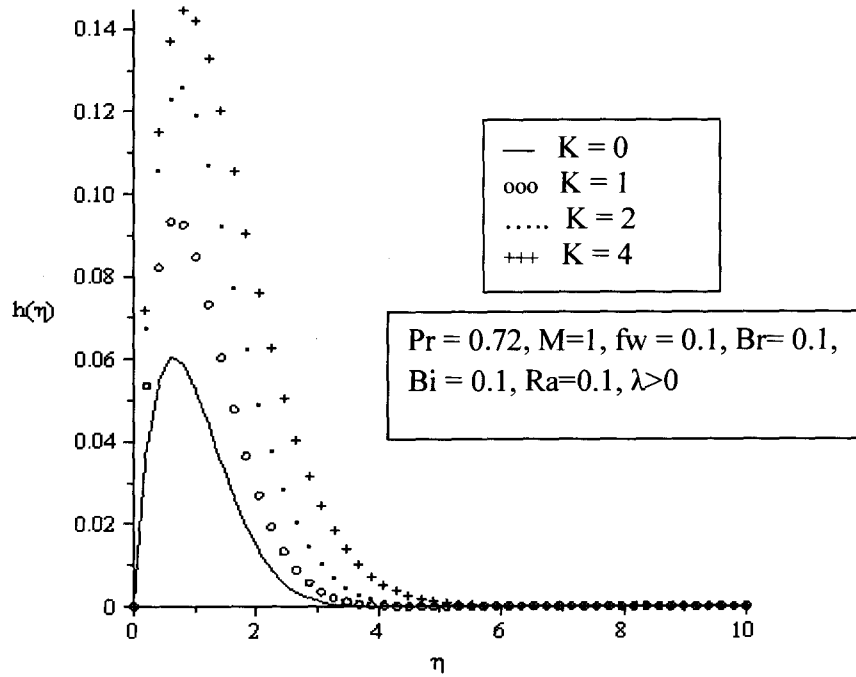


Figure 4. 11: Microrotation profiles for varying values of vortex viscosity parameter (assisting flow)

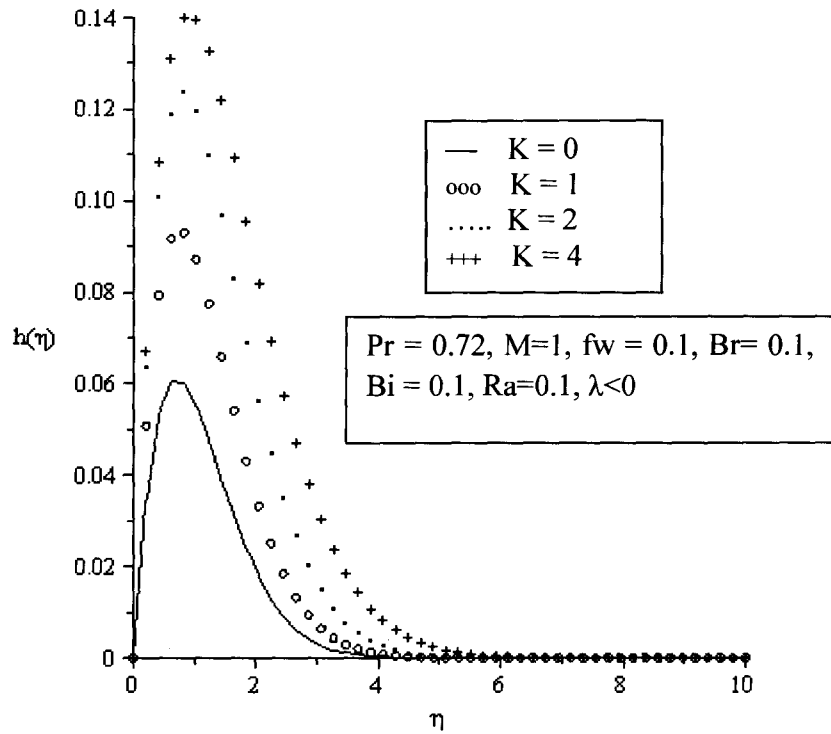


Figure 4. 12: Microrotation profiles for varying values of vortex viscosity parameter (opposing flow)



4.4.3 Temperature Profiles

The effects of parameter variation on temperature profiles are shown in Figures 4.13-4.21. Normally, the fluid temperature is highest at the surface of the plate and shrinks to free stream temperature satisfying the boundary conditions. It is observed from Figures 4.13-4.15 that increasing the magnetic field intensity slightly increases the thickness of the thermal boundary layer at the surface whereas increasing suction reduces the thermal boundary layer thickness.

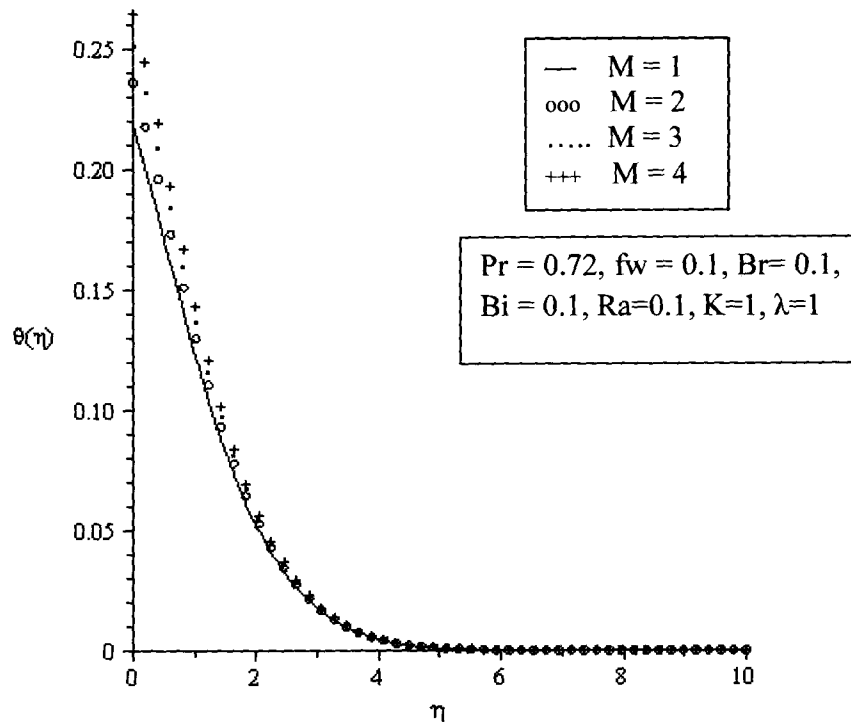


Figure 4. 13: Temperature profiles for varying values of magnetic field parameter

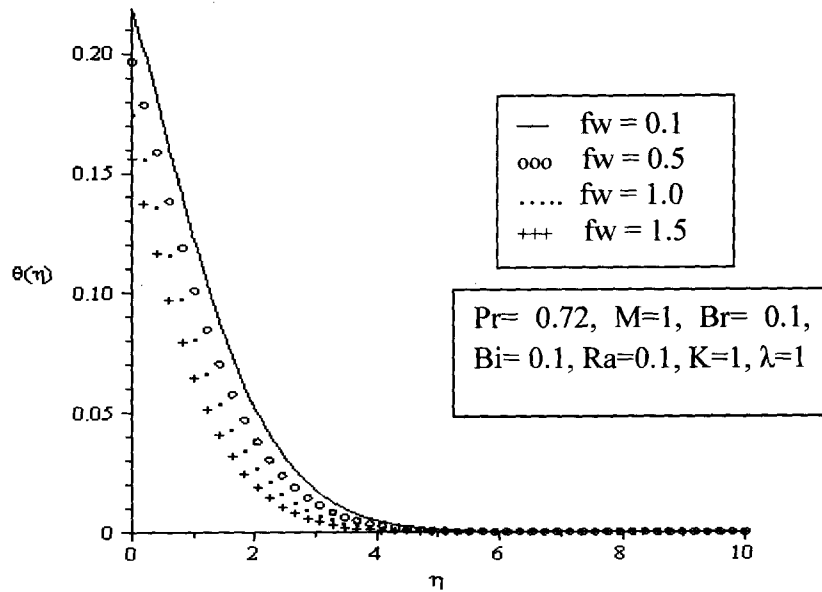


Figure 4. 14: Temperature profiles for varying values of suction parameter

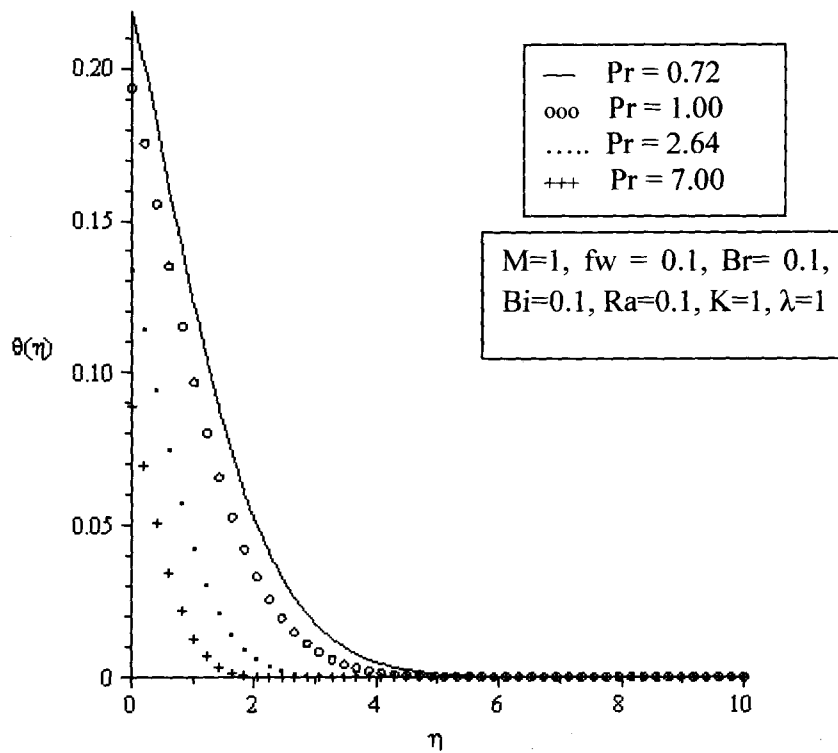


Figure 4. 15: Temperature profiles for varying values of the Prandtl number

Also, it is observed from Figure 4.16 that increasing values of the Prandtl number leads to a decrease in the thermal boundary layer thickness. This can be attributed to the fact that increasing Pr means increase in momentum diffusion over thermal diffusion and hence a decrease in the thermal boundary layer thickness at the surface. Meanwhile, from Figures 4.16-4.18, it is observed that increasing the intensity of viscous dissipation and convective heat transfer increase the temperature profiles.

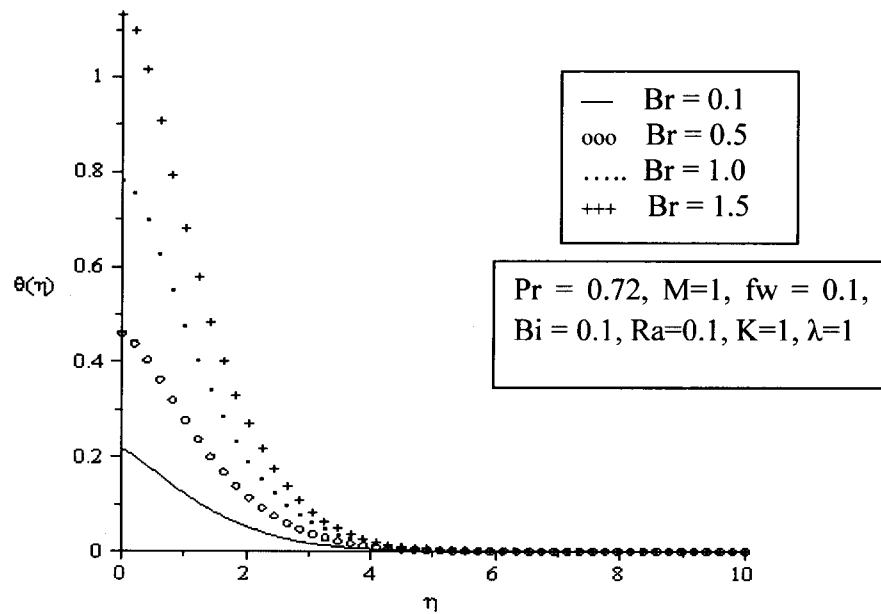


Figure 4. 16: Temperature profiles for varying values of the Brinkman number

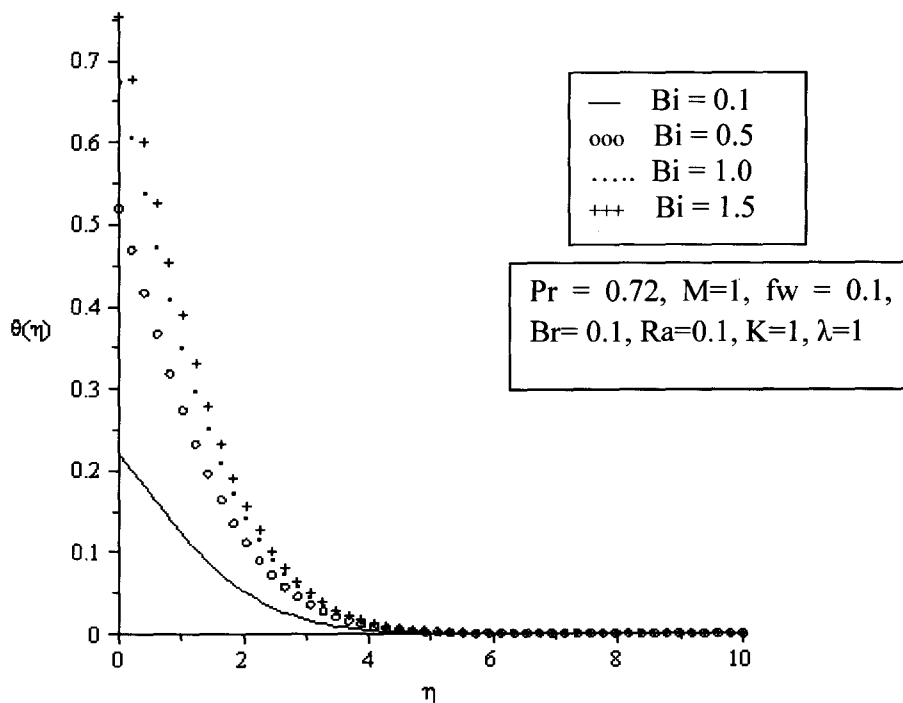


Figure 4. 17: Temperature profiles for varying values of Biot number

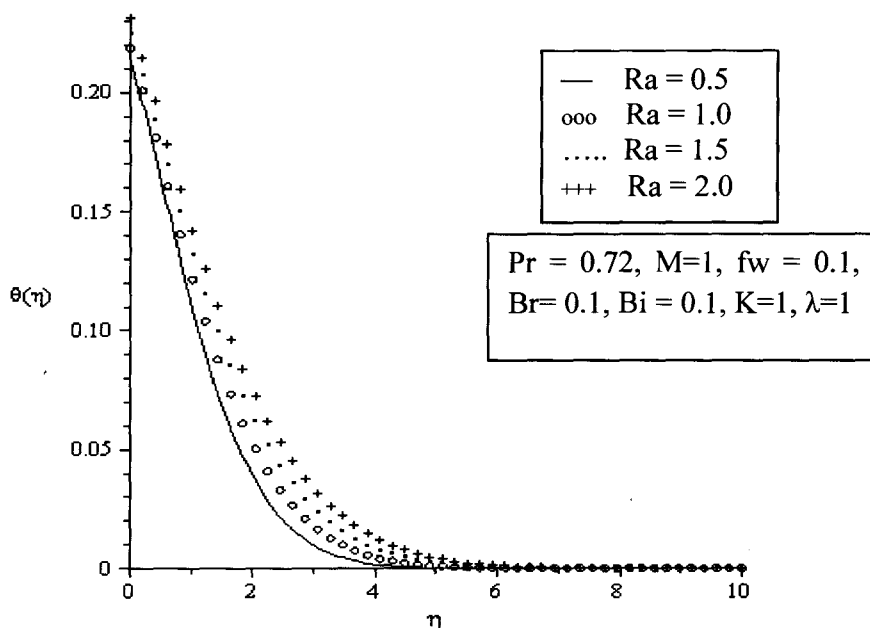


Figure 4. 18: Temperature profiles for varying values of the radiation parameter

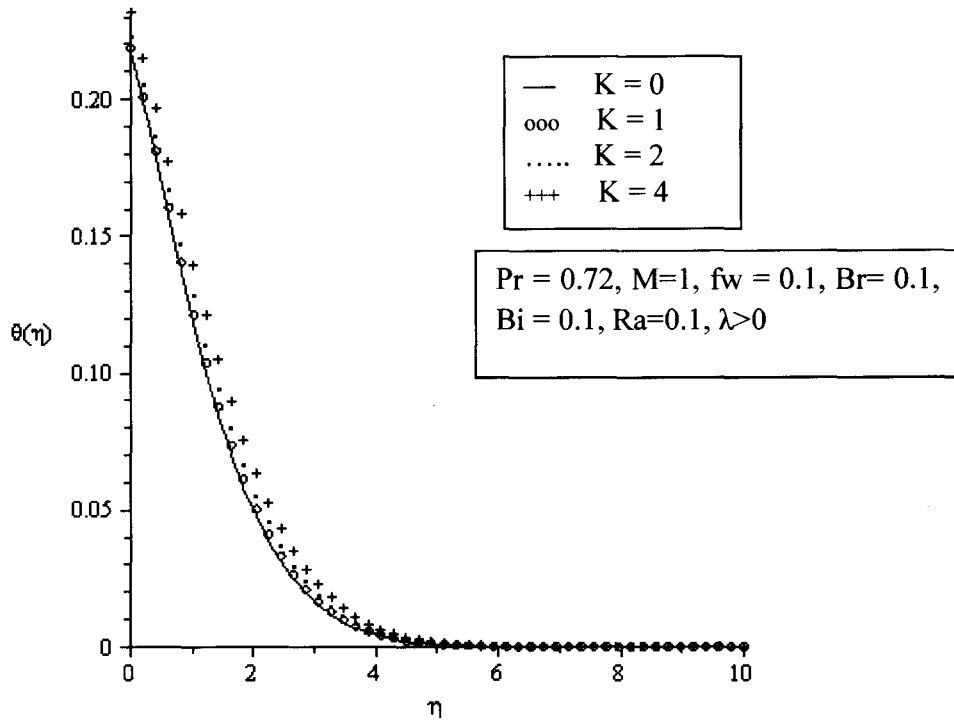


Figure 4. 19: Temperature profiles for varying values of material parameter (assisting flow)

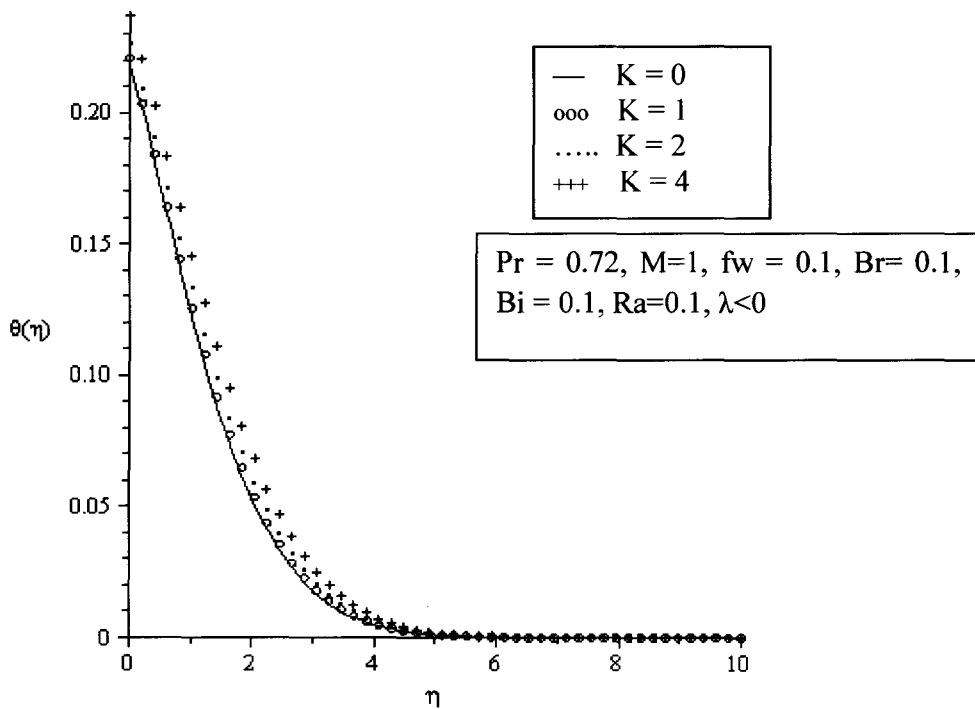


Figure 4. 20: Temperature profiles for varying values of material parameter (opposing flow)

This is due to the fact that as more heat is generated within the fluid, the fluid temperature increases leading to a sharp inclination of the temperature gradient between the plate surface and the fluid.

Moreover, Figures 19-20 show that increasing the vortex viscosity parameter for both assisting and opposing flows increases the thermal boundary layer thickness resulting into greater flow resistance (especially for assisting flow) in the boundary layer, thus reducing the rate at which heat is convected by the fluid. This, in turn, increases the fluid temperature in the neighbourhood of the plate surface causing the heat transfer rate at the wall to deteriorate. This influence of the micropolar structure of the fluid may be beneficial in the flow and temperature control of polymeric processing.



CHAPTER FIVE

CONCLUSIONS AND RECOMMENDATIONS

5.0 Introduction

This chapter presents the summary of findings, conclusions and recommendations of the study.

5.1 Summary of Findings

The research primarily investigated the combined effects of thermal radiation, viscous dissipation and convective heating on MHD micropolar flow over a vertical surface with heat transfer and convective boundary conditions. The effects of controlling parameters on the shear stress, couple stress, the rate of heat transfers, velocity, microrotation and temperature profiles were examined.

The equations governing the fluid flow in general was derived and based on some assumptions, a mathematical model was developed for a Blasius flow of micropolar fluid past a flat surface with the associated boundary conditions. These models were observed to be nonlinear partial differential equations of higher order whose solution was not readily available. To make these partial differential equations solvable numerically, similarity analysis was employed to transformed these equations to ordinary differential equations, which were then reduced to a system of nonlinear ordinary differential equations. The nonlinear ordinary differential equations were solved by using the forth - order Runge-Kutta integration scheme along with the Newton Raphson algorithm on Maple 16 software.



5.2 Conclusions

- i. The thermal boundary layer thickness, which is associated with the rate of heat transfer increases with the Magnetic field strength, viscous dissipation, convective heating, radiation and the viscosity at the vortex due to the flow rotations.
- ii. The momentum diffusion, due to suction and increased viscosity dominated thermal diffusion resulting in a reduced thermal boundary layer.
- iii. The induced Lorenz force and suction can be employed to reduce the velocity of the flow as well as the thickness of the micro-rotation. It is also noteworthy that increasing the micro-rotation and temperature parameters tend to increase the momentum of the flow due to dominant buoyancy forces.
- iv. Increases in viscous dissipation and radiation have adverse effect on the rate of heat transfer whereas increasing convective heat transfer enhances the heat transfer process. On the other hand, the rate of mass transfer is enhanced by an increase in the Lorenz force and the microrotation parameters.
- v. The present of the magnetic field parameter and suction lead to a reduction in flow whereas the permeability increases the fluid velocity.
- vi. The rate of heat transfer at the surface of the plate can be controlled by permeability, suction and the magnetic field strength to achieve desired flow kinematics.





5.3 Recommendations

- i. Investigation of the effects of cooling and heating on MHD heat transfer revealed that for the convective heat flux boundary condition, heat transfer (and associated enhancement) is higher when flow temperature is higher. As the surface temperature increases, the heat transfer and the associated enhancement increases. These facts should be taken into account for the practical application of MHD in heat transfer device.
- ii. Textile manufacturing involves a crucial energy-intensive drying stage at the end of the process to remove moisture left from dye setting. It is recommended that, in the process of optimising heat transfer in the drying process, thermal radiation should be controlled.
- iii. In the design of plate fin exchangers, convective heat transfer parameter among other parameters, must be given considerate attention, since it enhances the heat transfer process.
- iv. In the process of heat transfer, viscous dissipation parameters must be controlled as it increases temperature.

5.4 Suggestion for further study

- i. In heat and mass transfer processes, the Soret and Dufour effects are neglected because they are smaller order of magnitude than the effects described by Fourier's and Fick's laws. Further research to include Soret and Dufour effects in the present study is recommended.
- ii. Flow of micropolar fluids on inclined surfaces is recommended as it represents general orientation of plate.

- iii. MHD micropolar fluids on curved surfaces and circular conduits will be an interesting area of research.



REFERENCES

- Abdou, M. A, Morley, N. B, Ying, A. Y, Wong, C. P. C, Mann, T., Tourville, S. and the US ITER Test Blanket Module Team (2007). Technical Plan and Cost Estimate Summary, *US ITER Test Blanket Module Program*, (Vol I), University of California Los Angeles Report, UCLA-FNT.
- Ahmadi, G. (1976). Self-similar solution of incompressible micropolar boundary layer flow over a semi- infinite plate. *International Journal of Engineering and Science*, 14, 639 – 646.
- Ali, N. and Hayat, T. (2008). Peristaltic flow of a micropolar fluid in an asymmetric channel, *Computer & Mathematics with Applications*, 55(4), 589-608.
- Ariman, T., Turk, M.A. and Sylvester, N.D. (1974). Microcontinuum fluid mechanics – a review. *International Journal of Engineering and Science*, 12, 273-293.
- Arthur, E. M., Seini, Y.I. and Seidu, A., (2014). On Chemically Reacting Hydromagnetic Flow over a Flat Surface in the Presence of Radiation with Viscous Dissipation and Convective Boundary Conditions. *American Journal of Applied Mathematics*, 2(5), 179-185.
- Arthur, E.M., and Seini, Y.I. (2014). MHD Thermal Stagnation Point Flow towards a Stretching Porous Surface. *Mathematical Theory and Modeling*, 4(5), 163-169.
- Blasius, H. (1908). Gren zschichten in Fllissigkeiten mit kleiner Reibung, *Zeitschrift flir*
- Christian, E.J., Seini, Y.I. and Arthur, E. M. (2014). MHD boundary Layer stagnation point flow with Radiation and Chemical Reaction towards a Heated Shrinking Porous Surface. *International Journal of Physical Sciences*, 9(14), 320-328.

- Eringen, A.C. (1964). Simple microfluids. *International Journal of Engineering and Science*, 2, 205 -217
- Eringen, A.C. (1965). Theory of micropolar continua. *Proceedings of the Ninth Midwestern Conference*, 23
- Eringen, A. C. (1966). Theory of micropolar fluids. *Journal of Mathematical Mechanics*, 16, 1-18.
- Eringen, A.C.,(2001). Microcontinuum field theories II: Fluent media, *Springer*, Newyork.
- Hadimoto, B. and Tokioka, T. (1969). Two dimensional shear flows of linear micropolar fluids, *International Journal of Engineering and Science*, 7, 515-522.
- Hayat, T. and Ali, N. (2008). Effects of an endoscope on peristaltic of a micropolar fluid, *Mathematical and Computer Modelling*, 48(5-6), 721-733.
- Hayat, T., Abbas, Z. and Javed, T. (2008). Mixed convection flow of a micropolar fluid over a non-linearly stretching sheet. *Physics Letters A*, 372(5) 637-647.
- Hayat, T., Javed, T. and Abbas, Z. (2009). MHD flow of a micropolar fluid near a stagnation-point towards a non- linear stretching surface, *Nonlinear Analysis. Real World Application*, 10(3), 1514-1526.
- Hiemenz, K. (1911). Die Grenzschicht an einem in den gleichformigen Flussigkeitsstrom eingetauchten graden Kreiszyylinder. *Dinglers Polytech. J.*, 326, 321-324.
- Homann, F. (1936). Der Einfluss grosser Zahigkeit bei der Stromung um den Zylinder und um die Kugel. *Mathematik und Physik*, 56(1).
- Hoyt, J.W and Fabula, A. G. (1964). The effects of Additives on fluid friction. *U.S Naval*



Ordinance Test Station Report.

- Ibrahim, S.Y. and Makinde, O.D. (2011). Chemically reacting Magnetohydrodynamics (MHD) boundary layer flow of heat and mass transfer past a low-heat-sheet moving vertically downwards, *Scientific Research and Essays*, 6(22), 4762-4775.
- Imoro, R., Arthur, E.M. and Seini, Y.I. (2014). Heat and mass transfer over a vertical surface with convective boundary conditions in the presence of viscous dissipation and nth order chemical reaction. *International Journal of Computational and Applied Mathematics*, 9(2), 101-118.
- Ishak, A., Nazar, R. and Pop, I. (2008). Magnetohydrodynamics (MHD) flow of a micropolar fluid towards a stagnation point on a vertical surface. *Computers and Mathematics with Applications*, 56, pp. 3188-3194.
- Jovanovic, J., Frohnafel, B., Skaljic E., and Jovanovic, M. (2006). Persistence of the laminar regime in a flat plate boundary layer at very high Reynolds number. *Thermal Science*, 10.
- Lakshmi, M. P., Reddy, N. B., and Poornima, T. (2012). MHD Boundary Layer Flow of Heat and Mass Transfer over a Moving Vertical Plate in a Porous Medium with Suction and Viscous Dissipation. *International Journal of Engineering Research and Applications (IJERA)*, 2(5), pp. 149-159, ISSN: 2248-9622.
- Lockwood, F., Benchaitra, M. and Friberg, S. (1987). Study of polytropic liquid crystals in viscometric flow and elastohydrodynamic contact, *ASLE Tribology Trans.*, 30, 539- 548.
- Lok, Y.Y., Amin, N., Campean, D., Pop, I. (2005). Steady mixed convection flow of a



micropolar fluid near the stagnation point on a vertical surface, *Int. J.*

Numerical Methods Heat Flow 15, 654-670.

Mahapatra, T. R. and Gupta, A. S. (2002). Heat transfer in stagnation-point towards a stretching sheet. *International Journal of Engineering and Science*, 38, 517-521.

Makinde, O. D. (2011). Similarity solution for natural convection from a moving vertical plate with internal heat generation and a convective boundary condition, *Therm. Sci.*, 15(1), 137-143.

Nazar, R., Amin, N., Filip, D. and Pop, I. (2004). Stagnation point flow of a micropolar fluid towards a stretching sheet. *Int. J. of Non-Linear Mechanics*, 39(7), 1227-1235.

Neil B. M. and Mark S. T. (1993). Examination of stability calculations for liquid metal film flows in a coplanar magnetic field. *Magnetohydrodynamics*, 29(2).

Ostrach, S., (1952). An Analysis of Laminar Free-Convection Flow and Heat Transfer About a Flat Plate Parallel to the Direction of the Generating Body Force," *National Advisory Committee for Aeronautics Technical Note*, (2635).

Patel, M. and Timol, M. (2011). Magnetohydrodynamic orthogonal stagnation point flow of a power law fluid toward a stretching surface. *American Journal of Computer and Mathematics*, 1, 129-133.

Pop, S. R., Grosan, T. and Pop, I. (2004). Radiation effects on the flow near the stagnation point of a stretching sheet. *Tech. Mech.*, 25(2), 100-106.

Prandtl L (1904). U"ber Flu"ssigkeitsbewegung bei sehr kleiner Reibung.

Verhandlungen es 3 *Internationalen Mathematiker-Kongresses Heidelberg.*

Teubner, Leipzig, S 484-491

Pradeep, D. S. and Hussain, F. (2001). Core dynamics of strained vortex: instability and



transition, *J. Fluid Mech.*, 447, 247-285.

- Rajput, U. S. and Sahu, P.K., (2011). Combined Effect of MHD and Radiation on Unsteady Transient Free Convection Flow between two Long Vertical Parallel Plates with Constant Temperature and Mass Diffusion. *Gen. Math. Notes*, 6(1), 25-39, ISSN 2219-7184.
- Ramachandran, N., Chem, T. S. and Armaly, B.F. (1988). Mixed convection in a Stagnation flows adjacent to a vertical surfaces. *ASME J. Heat Mass Transfer*, 110, 373-377.
- Rees, D. A. S. and Pop, I.(1998). Free convection boundary layer flow of micropolar fluid from a vertical flat plate. *IMA J. Appl. Math.*, 61, pp. 179-197.
- Sajid, M., Abbas, Z. and Hayat, T. (2009). Homotopy analysis for boundary layer flow of a micropolar fluid through a porous channel. *Applied Mathematical Modelling*, 33(11), 4120-4125.
- Soundalgekar, V. M. and Takhar, H. S. (1983). Flow of a micropolar fluid on a continuous moving plate, *International Journal of Engineering Science*, 21, 961.
- Sparrow, E. M., Cess R. D. and Timol, M. (1961). Effect of magnetic field on free Convection heat transfer, *International Journal of Heat and Mass Transfer*, 3, 267-270
- Subhas, M. A., Sanjayanand, E., and Mahantesh, M. N. (2007). Viscoelastic MHD flow and heat transfer over a stretching sheet with viscous and Ohmic dissipation, *Comms in Nonlinear Science and Numerical Simulation*, 13, 1808– 1821.
- Zhu, J., Zheng, L.C., Zhang, X. X. (2011). The influence of thermal radiation on MHD



stagnation point flow past a stretching sheet with heat generation. *Acta. Mech. Sin.*, 27(4), 502-509.



APPENDICES

APPENDIX I

Fourth order Runge-Kutta and Newton-Raphson's algorithms

i. The Fourth order Runge-Kutta Formula.

$$k_1 = hf(x_n, y_n)$$

$$k_2 = hf\left(x_n + \frac{h}{2}, y_n + \frac{k_1}{2}\right)$$

$$k_3 = hf\left(x_n + \frac{h}{2}, y_n + \frac{k_2}{2}\right)$$

$$k_4 = hf(x_n + h, y_n + k_3)$$

$$y_{n+1} = y_n + \frac{k_1}{6} + \frac{k_2}{3} + \frac{k_3}{3} + \frac{k_4}{6} + O(h^5)$$

Where h is the step size.

ii. The Newton-Raphson's formula.

$$x_1 = x_0 - \frac{f(x_0)}{f'(x_0)}$$

$$x_{i+1} = x_i - \frac{f(x_i)}{f'(x_i)}$$

Where x_0 is an initial guess.



APPENDIX II

Maple code for numerical results

```
> Pr := 10 : M := 0 : K := 0 : lambda := 1 : Ra := 0 : Br := 0 : Bi
:= 1000000 : fw := 0 :
```

```
fens := {F(y), theta(y), h(y)} :
```

```
sys1 := (1 + K) · diff(F(y), y$3) + F(y) · diff(F(y), y$2) + M · (1
- diff(F(y), y)) - diff(F(y), y)^2 + lambda · theta(y) + K · diff(h(y), y) =
-1, (1 + 4/3 · Ra) · diff(theta(y), y$2) + Pr · F(y) · diff(theta(y), y)
- Pr · theta(y) · diff(F(y), y) + Br · (diff(F(y), y$2))^2 = 0, (1
+ K/2) · diff(h(y), y$2) + F(y) · (diff(h(y), y)) - diff(F(y),
y) · h(y) - K(2 · h(y) + diff(F(y), y$2)) = 0, D(F)(0) = 0,
F(0) = fw, h(0) = -1/2 · F''(0), D(theta)(0) = Bi · (theta(0) - 1),
D(F)(10) = 1, theta(10) = 0, h(10) = 0 :
```

$$\frac{d^3}{dy^3} F(y) + F(y) \left(\frac{d^2}{dy^2} F(y) \right) - \left(\frac{d}{dy} F(y) \right)^2 + \theta(y) = -1,$$

$$\frac{d^2}{dy^2} \theta(y) + 10 F(y) \left(\frac{d}{dy} \theta(y) \right) - 10 \theta(y) \left(\frac{d}{dy} F(y) \right) = 0,$$

$$\frac{d^2}{dy^2} h(y) + F(y) \left(\frac{d}{dy} h(y) \right) - \left(\frac{d}{dy} F(y) \right) h(y) = 0,$$

$$D(F)(0) = 0, F(0) = fw, h(0) = -\frac{1}{2} D^{(2)}(F)(0), D(\theta)(0) = Bi \cdot (\theta(0) - 1)$$

$$= 1000000\theta(0) - 1000000 D(F)(10) = 1, \theta(10) = 0, h(10) = 0$$

```
p := dsolve( { sys1, D(F)(0) = 0, F(0) = fw, h(0) = -1/2 · F''(0),
D(theta)(0) = Bi · (theta(0) - 1), D(F)(10) = 1, theta(10) = 0, h(10) = 0 },
fens, type = numeric, method = bvp, abserr = 0.000001)
```

```
proc(x_bvp) ... end proc
```



dsoll := *dsolve* ({*sys1*}, *numeric*, *output* = *operator*)

```
[y = proc(y) ... end proc, F = proc(y) ... end proc, D(F) =  
  proc(y)  
  ...  
end proc, D(2)(F) = proc(y) ... end proc, h = proc(y)  
  ...  
end proc, D(h) = proc(y) ... end proc, θ = proc(y) ... end proc,  
  D(θ) = proc(y) ... end proc ]
```

dsoll (0);

```
[y = 0, F(0) = 0., D(F) (0) = 0., D(2)(F) (0) = 1.49283818231836896  
  h(0) = -0.746419091159184478  
  D(h) (0) = 0.6230697146569500478  
  θ(0) = 0.999998055386536744  
  D(θ) (0) = -1.94461346293421688
```



APPENDIX III

Maple code for graphical results

```

> Pr := 0.72 : M := 1 : K := 1 : λ := 1 : Ra := 1 : Br := 0.1 : Bi
   := 0.1 : fw := 0.1 :

fcns := {F(y), θ(y), h(y)} :

sys := (1 + K) · diff(F(y), y$3) + F(y) · diff(F(y), y$2) + M · (1
- diff(F(y), y) - diff(F(y), y)2 + λ · θ(y) + K · diff(h(y), y) =
-1, (1 +  $\frac{4}{3}$  · Ra) · diff(θ(y), y$2) + Pr · F(y) · diff(θ(y), y)
- Pr · θ(y) · diff(F(y), y) + Br · (diff(F(y), y$2))2 + M
· Br · (1 - diff(F(y), y))2 = 0, (1 +  $\frac{K}{2}$ ) · diff(h(y), y$2)
+ F(y) · (diff(h(y), y) - diff(F(y), y) · h(y) + K · (-2 · h(y)
+ diff(F(y), y$2)) = 0 :

p1 := dsolve({ sys, D(F)(0) = 0, F(0) = fw, h(0) = - $\frac{1}{2}$  · F''(0),
D(θ)(0) = Bi · (θ(0) - 1), D(F)(10) = 1, θ(10) = 0, h(10) = 0 },
fcns, type = numeric, method = bvp, abserr = 1e-6)

proc(x_bvp) ... end proc

p1f := odeplot(p1, [y, F'(y)], 0..10, numpoints = 50, labels = ["η",
"F'(η)"], style = patch, symbol = asterisk, color = black) :

p1t := odeplot(p1, [y, θ(y)], 0..10, numpoints = 50, labels = ["η",
"θ(η)"], style = patch, symbol = asterisk, color = black) :

p1c := odeplot(p1, [y, h(y)], 0..10, numpoints = 50, labels = ["η",
"h(η)"], style = patch, symbol = asterisk, color = black) :

with(plots) :

Pr := 0.72 : M := 1 : K := 1 : λ := 1 : Ra := 1 : Br := 0.1 : Bi
   := 0.1 : fw := 0.1 :

fcns := {F(y), θ(y), h(y)} :

```



$$\begin{aligned} \text{sys} := & (1 + K) \cdot \text{diff}(F(y), y\$3) + F(y) \cdot \text{diff}(F(y), y\$2) + M \cdot (1 \\ & - \text{diff}(F(y), y)) - \text{diff}(F(y), y)^2 + \lambda \cdot \theta(y) + K \cdot \text{diff}(h(y), y) = \\ & -1, \left(1 + \frac{4}{3} \cdot Ra\right) \cdot \text{diff}(\theta(y), y\$2) + Pr \cdot F(y) \cdot \text{diff}(\theta(y), y) \\ & - Pr \cdot \theta(y) \cdot \text{diff}(F(y), y) + Br \cdot (\text{diff}(F(y), y\$2))^2 + M \\ & \cdot Br \cdot (1 - \text{diff}(F(y), y))^2 = 0, \left(1 + \frac{K}{2}\right) \cdot \text{diff}(h(y), y\$2) \\ & + F(y) \cdot (\text{diff}(h(y), y)) - \text{diff}(F(y), y) \cdot h(y) + K \cdot (-2 \cdot h(y) \\ & + \text{diff}(F(y), y\$2)) = 0 : \end{aligned}$$

$$\begin{aligned} p2 := & \text{dsolve} \left(\left\{ \text{sys}, D(F)(0) = 0, F(0) = fw, h(0) = -\frac{1}{2} \cdot F''(0), \right. \right. \\ & \left. \left. D(\theta)(0) = Bi \cdot (\theta(0) - 1), D(F)(10) = 1, \theta(10) = 0, h(10) = 0 \right\}, \right. \\ & \left. \text{fcns}, \text{type} = \text{numeric}, \text{method} = \text{bvp}, \text{abserr} = 1e-6 \right) \end{aligned}$$

proc(x_bvp) ... end proc

$$\begin{aligned} > p2f := & \text{odeplot}(p2, [y, F'(y)], 0..10, \text{numpoints} = 50, \text{labels} = ["\eta", \\ & "F'(\eta)"], \text{style} = \text{point}, \text{symbol} = \text{circle}, \text{color} = \text{black}) : \end{aligned}$$

$$\begin{aligned} > p3 := & \text{dsolve} \left(\left\{ \text{sys}, D(F)(0) = 0, F(0) = fw, h(0) = -\frac{1}{2} \cdot F''(0), \right. \right. \\ & \left. \left. D(\theta)(0) = Bi \cdot (\theta(0) - 1), D(F)(10) = 1, \theta(10) = 0, h(10) = 0 \right\}, \right. \\ & \left. \text{fcns}, \text{type} = \text{numeric}, \text{method} = \text{bvp}, \text{abserr} = 1e-6 \right) \end{aligned}$$

proc(x_bvp) ... end proc

$$\begin{aligned} p3f := & \text{odeplot}(p3, [y, F'(y)], 0..10, \text{numpoints} = 50, \text{labels} = ["\eta", \\ & "F'(\eta)"], \text{style} = \text{point}, \text{symbol} = \text{point}, \text{color} = \text{black}) : \end{aligned}$$

$$\begin{aligned} p3t := & \text{odeplot}(p3, [y, \theta(y)], 0..10, \text{numpoints} = 50, \text{labels} = ["\eta", \\ & "\theta(\eta)"], \text{style} = \text{point}, \text{symbol} = \text{point}, \text{color} = \text{black}) : \end{aligned}$$

$$\begin{aligned} p3c := & \text{odeplot}(p3, [y, h(y)], 0..10, \text{numpoints} = 50, \text{labels} = ["\eta", \\ & "h(\eta)"], \text{style} = \text{point}, \text{symbol} = \text{point}, \text{color} = \text{black}) : \end{aligned}$$

with(plots) :



```
Pr := 0.72 : M := 1 : K := 1 : λ := 1 : Ra := 1 : Br := 0.1 : Bi
:= 0.1 : fw := 0.1 :
```

```
fcns := {F(y), θ(y), h(y)} :
```

```
sys := (1 + K) · diff(F(y), y$3) + F(y) · diff(F(y), y$2) + M · (1
- diff(F(y), y)) - diff(F(y), y)2 + λ · θ(y) + K · diff(h(y), y) =
-1, (1 +  $\frac{4}{3}$  · Ra) · diff(θ(y), y$2) + Pr · F(y) · diff(θ(y), y)
- Pr · θ(y) · diff(F(y), y) + Br · (diff(F(y), y$2))2 + M
· Br · (1 - diff(F(y), y))2 = 0, (1 +  $\frac{K}{2}$ ) · diff(h(y), y$2)
+ F(y) · (diff(h(y), y)) - diff(F(y), y) · h(y) + K · (-2 · h(y)
+ diff(F(y), y$2)) = 0 :
```

```
p4 := dsolve( { sys, D(F)(0) = 0, F(0) = fw, h(0) = - $\frac{1}{2}$  · F''(0),
D(θ)(0) = Bi · (θ(0) - 1), D(F)(10) = 1, θ(10) = 0, h(10) = 0 },
fcns, type = numeric, method = bvp, abserr = 1e-6 )
```

```
proc(x_bvp) ... end proc
```

```
p4f := odeplot(p4, [y, F'(y)], 0..10, numpoints = 50, labels = ["η",
"F'(η)"], style = point, symbol = cross, color = black) :
```

```
p4t := odeplot(p4, [y, θ(y)], 0..10, numpoints = 50, labels = ["η",
"θ(η)"], style = point, symbol = cross, color = black) :
```

```
p4c := odeplot(p4, [y, h(y)], 0..10, numpoints = 50, labels = ["η",
"h(η)"], style = point, symbol = cross, color = black) :
```

```
> plots[display]({p1f, p2f, p3f, p4f});
```